Title

Quantification of brain oxygen extraction and metabolism with [15O]-gas PET: A technical review in the era of PET/MRI

Authors

Fan, Audrey P
An, Hongyu
Moradi, Farshad
et al.

Publication Date

2020-10-01

DOI

10.1016/j.neuroimage.2020.117136

Peer reviewed

Published in final edited form as:

Neuroimage. 2020 October 15; 220: 117136. doi:10.1016/j.neuroimage.2020.117136.

Quantification of brain oxygen extraction and metabolism with [^{15}O]-gas PET: A technical review in the era of PET/MRI

Audrey P. Fan[a,b,*], **Hongyu An**[c], **Farshad Moradi**[a], **Jarrett Rosenberg**[a], **Yosuke Ishii**[a,d], **Tadashi Nariai**[d], **Hidehiko Okazawa**[e], **Greg Zaharchuk**[a]

[a]Department of Radiology, Stanford University, Stanford, CA, USA

[b]Department of Biomedical Engineering and Department of Neurology, University of California Davis, Davis, CA, USA

[c]Department of Radiology, Washington University in St. Louis, St. Louis, MO, USA

[d]Department of Neurosurgery, Tokyo Medical and Dental University, Tokyo, Japan

[e]Biomedical Imaging Research Center, University of Fukui, Fukui, Japan

Abstract

Oxygen extraction fraction (OEF) and the cerebral metabolic rate of oxygen ($CMRO_2$) are key cerebral physiological parameters to identify at-risk cerebrovascular patients and understand brain health and function. PET imaging with [^{15}O]-oxygen tracers, either through continuous or bolus inhalation, provides non-invasive assessment of OEF and $CMRO_2$. Numerous tracer delivery, PET acquisition, and kinetic modeling approaches have been adopted to map brain oxygenation. The purpose of this technical review is to critically evaluate different methods for [^{15}O]-gas PET and its impact on the accuracy and reproducibility of OEF and $CMRO_2$ measurements. We perform a meta-analysis of brain oxygenation PET studies in healthy volunteers and compare between continuous and bolus inhalation techniques. We also describe OEF metrics that have been used to detect hemodynamic impairment in cerebrovascular disease. For these patients, advanced techniques to accelerate the PET scans and potential synthesis with MRI to avoid arterial blood sampling would facilitate broader use of [^{15}O]-oxygen PET for brain physiological assessment.

Keywords

Oxygen extraction fraction; Cerebral metabolic rate of oxygen; Positron emission tomography; [^{15}O]-oxygen

*Corresponding author. Department of Biomedical Engineering and Department of Neurology, University of California, Davis, 1590 Drew Avenue Unit 1, Davis, CA, 95618, USA. apfan@ucdavis.edu (A.P. Fan).

Declaration of competing interest

All authors report no disclosures and no conflicts of interest related to the topic of this manuscript.

Data availability statement

Data sheets for the healthy volunteer studies reviewed in this manuscript, as well as the STATA script for statistical meta-analysis are uploaded to an open repository: https://github.com/fanlab-ucdavis/O15gas-PET.git.

1. Introduction

The human brain has an impressively high metabolic demand, consuming 20% of total oxygen used by the body (Magistretti and Pellerin, 1996; Gallagher et al., 1998), and suffers devastating consequences when this oxygen supply is disrupted. Impaired oxygen metabolism is a hallmark of stroke (Ackerman et al., 1981; Marchal et al., 1999; Baron et al., 1981), traumatic brain injury (Coles et al., 2004; Vespa et al., 2005), and tumors (Lammertsma et al., 1985; Ogawa et al., 1988), and is likely present in early neurodegeneration (Ishii et al., 1996). The ability to non-invasively image oxygen extraction fraction (OEF) in the brain and the cerebral metabolic rate of oxygen ($CMRO_2$) has tremendous clinical value. In neurovascular disease, regional OEF assessment can identify acute stroke patients with viable tissue who stand to benefit from new revascularization treatments (Menon et al., 2015), particularly if they fall outside the established treatment guidelines (Albers et al., 2018). For investigations of neurocognitive processes (Fox and Raichle, 1986; Mintun et al., 2001), $CMRO_2$ is the main parameter of interest as it is more robust than OEF to physiological variability, e.g. due to vasoactive substances such as medications or caffeine.

Although PET imaging with [^{15}O]-gas tracers is considered the reference standard for OEF and $CMRO_2$ measurements, past studies have adopted widely different approaches. Methodological sources of variability include radiotracer and delivery approach, PET scanner, image reconstruction, and model analysis. Understanding how methodological choices impact the accuracy and reliability of PET oxygenation estimates is critical to interpretation of these studies. While other reviews have nicely summarized the historical development of [^{15}O]-gas PET (Baron and Jones, 2012) and its clinical impact (Okazawa and Kudo, 2009), this paper focuses on the technical considerations to measuring OEF and $CMRO_2$ with [^{15} O]-oxygen. Recent approaches to quantify brain oxygenation without invasive arterial blood sampling and with shorter scan time are discussed. Semi-quantitative methods are compared for their efficacy to identify impaired OEF in patients with cerebrovascular disease. Finally, opportunities to leverage multi-modal imaging on simultaneous PET/MRI scanners to validate new, non-invasive oxygenation imaging methods are highlighted.

2. Theory for brain oxygenation imaging with [^{15}O]-gas PET

2.1. [^{15}O]-oxygen kinetic model

The key radiotracer to measure oxygen metabolism is [^{15}O]-oxygen, which is breathed by the patient through continuous gas inhalation over a period of minutes, or through bolus inhalation. After [^{15}O]-oxygen exchanges in the lungs and enters into the bloodstream, it is delivered by arterial blood (primarily bound to hemoglobin) to the brain. In the capillary bed, [^{15}O]-oxygen is extracted from the vasculature into cerebral tissues, which is modeled by a single-tissue kinetic model (Mintun et al., 1984; Subramanyam et al., 1978) (Fig. 1a). This oxygen extraction is characterized by the percent OEF (a key parameter of interest) and is assumed to occur instantaneously (Subramanyam et al., 1978). Aerobic metabolic processes in brain tissues then convert [^{15}O]-oxygen to metabolic [^{15}O]-water, which also recirculates throughout the body. The presence of dissolved [^{15}O]-oxygen in both the blood

and tissue compartments is negligible compared to [^{15}O]-oxygen bound to hemoglobin and the [^{15}O]-water metabolites (Frackowiak et al., 1980). During the imaging experiment, the temporal dynamics of these radiolabeled compounds depend on the delivery method for the [^{15}O]-oxygen tracer. For the continuous method, temporal dynamics are mostly ignored, whereas for the bolus method, kinetic modeling aims to dissociate the effects of $CMRO_2$ and CBF on the temporal PET curve.

2.2. Continuous versus bolus gas inhalation

Two primary delivery approaches, continuous gas inhalation and bolus inhalation, have been used for [^{15}O]-oxygen PET. The initial studies adopted continuous inhalation of [^{15}O]-oxygen over several half-lives of the tracer so that the arterial (supply) and recirculation concentrations of [^{15}O]-oxygen and [^{15}O]-water reach equilibrium (Subramanyam et al., 1978; Frackowiak et al., 1980). PET acquisition commences after this steady-state is achieved, and OEF and oxygen metabolism are assumed constant over the measurement period. Typical delivery flow rates are 0.5 L/min for 8–10 min before the start of imaging (Lenzi et al., 1981; Yamaguchi et al., 1986; Senda et al., 1988), which continues during the PET scan. The [^{15}O]-oxygen dose delivered ranges from 400 to 2253 MBq/min during the experiment (Frackowiak et al., 1980; Leenders et al., 1990), resulting in total of up to 6.4–51.8 GBq inhaled by the patient. Tracer activity and flow rate are monitored so that the concentration of the delivered gas tracer varies only by 2–3% (Frackowiak et al., 1980; Yamaguchi et al., 1986). Physiological equilibrium can be confirmed by monitoring a total-head radioactivity curve with the PET detectors (Yamaguchi et al., 1986). Different breathing apparatus can be used for continuous [^{15}O]-oxygen inhalation, which include light, disposable face masks (Frackowiak et al., 1980; Leenders et al., 1990); a standard oxygen mask with nasal cannula (Lebrun--Grandie et al., 1983); and a mouthpiece with a one-way valve (Subramanyam et al., 1978).

In contrast, bolus inhalation of [^{15}O]-oxygen has become more prevalent in recent decades. In this paradigm, [^{15}O]-oxygen is delivered through a short inhalation of up to 1 min (Mintun et al., 1984; Maeda et al., 2015; Shidahara et al., 2002), or through a single deep breath (Meyer et al., 1987; Ohta et al., 1992), e.g. with a 10-s breath hold. Because the necessary volume of gas tracer is smaller for bolus experiments, the [^{15}O]-oxygen can be supplied from the cyclotron and contained in a lead-shielded respiration bag (Ohta et al., 1992), and ultimately breathed by the subject through a short ventilator hose. The typical [^{15}O]-oxygen bolus dose is considerably lower than for continuous inhalation (Table 1). For image acquisition, dynamic PET scans are started immediately with the [^{15}O]-oxygen inhalation to capture the tracer kinetics, or a static PET scan is performed up to 20 s after the start of bolus inhalation for autoradiography.

The main advantages of bolus over continuous inhalation of [^{15}O]-oxygen are lower radiation dose to the patient and shorter scan time (Fig. 2a). Due to the faster tracer delivery and reduced dose, bolus inhalation is more amenable to repeated, dynamic scans to assess OEF measurement reproducibility (Bremmer et al., 2011); different brain physiological states after pharmacological vasodilation (Okazawa et al., 2001a) or anesthesia (Kaisti et al., 2003); and oxygen consumption changes during functional brain activity (Fox and Raichle,

1986; Mintun et al., 2002). Although the steady-state method has favorable signal-to-noise ratio (SNR) and provides measurements that are less sensitive to kinetic model assumptions (Huang et al., 1986), the requirement that brain physiology remains constant throughout the experiment is limiting. Physiological drift during a 10-min scan leads to largest measurement error for low OEF conditions, and up to 10% total error under even in normal conditions if OEF drifts by 2% per minute (Correia et al., 1985). Furthermore, both instability in cyclotron output and normal variations in patient respiration rate lead to changes in arterial blood concentration of [^{15}O]-oxygen tracer. After reviewing over 600 studies, Lammertsma et al. identified the mean coefficient of variation for arterial radioactivity concentration to be 5%, resulting in OEF errors of up to 6% (Lammertsma et al., 1988). Improving the robustness of OEF to changes in arterial radioactivity requires more sophisticated models that do not assume physiological equilibrium (Senda et al., 1988). Even with reliable tracer delivery, steady-state OEF measurements are also more susceptible to errors from tissue heterogeneity, i.e. multiple tissue types and OEF values within a voxel (Correia et al., Fig. 5) (Correia et al., 1985). These tissue heterogeneity effects are most problematic at early time points (Huang et al., 1986) and for shorter PET time frames with increased noise (Kobayashi et al., 2008).

Okazawa et al. directly compared the bolus and continuous inhalation methods within the same scan session for 7 healthy volunteers (Okazawa et al., 2001b). No statistical differences in global OEF between the bolus (47.2 ± 4%) and steady-state approaches (43.6 ± 3%) were observed. Global $CMRO_2$ observed by the bolus method (3.19 ± 0.2 ml/100 g/min) was slightly higher than that observed by the steady-state method (2.87 ± 0.2 ml/100 g/min) (Okazawa et al., 2001b), particularly near major veins and sinuses, but the two methods were strongly correlated (Pearson R = 0.87). Based on this agreement, the authors suggested that the bolus method can simplify oxygen metabolism PET analysis while providing OEF and $CMRO_2$ maps that are comparable with the steady-state method. Remaining discrepancies between the techniques should be explored in future comparisons, with careful control for the PET acquisition, assumptions about recirculating water, and correction for blood volume in tissue voxels.

2.3. Cerebral blood flow and cerebral blood volume

Full quantification of OEF and $CMRO_2$ generally requires three separate PET scans with [^{15}O]-oxygen gas, [^{15}O]-water or [^{15}O]-CO_2 for blood flow, and [^{15}O]-CO for blood volume. Although Fig. 2a depicts a representative ordering of these scans within an experiment, the order of the three tracer administrations is not fixed. The range of radioactivity doses used for the auxiliary PET tracers are also summarized in Table 1. A separate PET scan of cerebral blood flow (CBF) is acquired during inhalation of [^{15}O]-CO_2 gas, which exchanges with water in the body through the carbonic anhydrase reaction. This reaction labels the exchanged water as a freely diffusible tracer to assess perfusion in vivo (Subramanyam et al., 1978). [^{15}O]-CO_2 is continuously inhaled for 8–10 min to reach steady-state before the start of PET scanning, similar to [^{15}O]-oxygen. Alternatively, [^{15}O]-water can be administered directly as a perfusion tracer through intravenous injection. PET acquisition starts immediately with the [^{15}O]-water bolus administration to provide dynamic frames for kinetic modeling or an autoradiographic scan (Hatazawa et al., 1995; Ibaraki et

al., 2008) of CBF. Technical aspects of perfusion measurement with [^{15}O]-water PET have been previously reviewed in detail (Fan et al., 2016; Zeisig et al., 2014).

The resulting CBF map is important for accurate quantification of OEF from [^{15}O]-oxygen PET. For steady-state [^{15}O]-oxygen experiments, the PET signal at equilibrium is proportional to both OEF and CBF (Lammertsma and Jones, 1983), so OEF calculation involves a division of the [^{15}O]-oxygen and [^{15}O]-CO_2 scans. On the other hand, the PET signal during bolus inhalation of [^{15}O]-oxygen has a more complex, time-dependent relationship with OEF and CBF, as described by Mintun et al. (1984). CBF information thus is an essential component of OEF mapping, and also enables subsequent calculation of $CMRO_2$ for each voxel as: $CMRO_2$ = CBF x OEF x (arterial blood O_2 content). In simulations, Huang et al. determined that the reliability of $CMRO_2$ values depends heavily on the CBF condition (Huang et al., 1986). For low CBF and low OEF, relatively little [^{15}O]-oxygen tracer is extracted into the tissue, leading to larger statistical noise and higher coefficient of variation of the $CMRO_2$ estimate (e.g., 10% compared to only 2% in normal flow and oxygenation conditions). Fig. 2b summarizes the reliability of $CMRO_2$ quantification for different physiological conditions.

The final necessary PET scan measures cerebral blood volume (CBV) using inhalation of [^{15}O]-CO gas (Grubb et al., 1978; Phelps et al., 1979). Because carbon monoxide binds favorably and irreversibly to hemoglobin in red blood cells, the tracer essentially acts as a blood pool agent. [^{15}O]-CO gas is inhaled for 1–3 min, frequently with a mixture of room air and oxygen, before a static PET acquisition lasting 2–3 min to assess CBV. Quantitative CBV calculation requires assumption of the regional-to-large vessel hematocrit ratio, as hematocrit is lower in the capillaries (85–88% (Okazawa et al., 1996)) than in large vessels. Although the first PET $CMRO_2$ measurements were performed without CBV information, ignoring CBV creates 10% $CMRO_2$ error in high flow conditions and up to 20% error in low flow conditions (Huang et al., 1986). When OEF or CBF is low, there is minimal tissue signal from labelled metabolic water during an [^{15}O]-oxygen PET experiment, and the presence of vascular, unextracted activity becomes comparatively important (Fig. 2b). This unextracted [^{15}O]-oxygen activity is prominent in large sinuses and surrounding tissues (Hatazawa et al., 1995), and leads to OEF overestimation by 14% in gray matter and 8% in white matter (Okazawa et al., 2001b; Lammertsma and Jones, 1983).

Lammertsma et al. proposed a CBV correction factor for OEF, which mitigates this bias and reduces the measurement coefficient of variation, especially for low OEF and CBF conditions (Lammertsma and Jones, 1983). This correction assumed that the blood volume measured using [^{15}O]-CO is purely venous, i.e. the venous fraction is 100%. However, for typical ranges of OEF, the intravascular radioactivity of [^{15}O]-O_2 will be different between arterial and venous vessels due to oxygen extraction. Therefore, the venous fraction of CBV should be assumed, and has been measured to be 80% in fixed tissue samples (Wiedeman, 1963). For some steady-state PET corrections, the dependency of CBV on the regional-to-large vessel hematocrit ratio cancels out because both [^{15}O]-oxygen and [^{15}O]-CO tracers are equally affected by changes in hematocrit (Lammertsma et al., 1987).

To accommodate the use of multiple [^{15}O]-PET tracers, most studies wait 7–10 min between the separate scans for the radioactivity to decay over several half-lives. If physiology changes between the scans, the error may be propagated to the final $CMRO_2$ estimate. The largest errors are expected for low flow and low OEF conditions, with 1% error propagation leading to 5% $CMRO_2$ bias (Huang et al., 1986). Eliminating one of the PET scans (e.g. by assuming a relationship between CBF and CBV and omitting the [^{15}O]-CO acquisition) could reduce errors due to changes in physiology and simplify the scan procedure. However, an accurate relationship between CBF and CBV may not be known for pathological conditions. Alternatively, the uncertainty introduced by the lack of direct CBV measurement could be mitigated by slightly increasing the [^{15}O]-oxygen dose. The resulting SNR gain would enable improved, simultaneous fits of multiple parameters (including blood volume) from dynamic PET, without increasing total radioactivity to the patient.

3. Methodological considerations for [^{15}O]-oxygen PET

3.1. PET scanner and image acquisition

Image acquisition for [^{15}O]-PET experiments has varied widely in scanner hardware and spatial resolution. Early 2-dimensional (2D) PET imaging was limited in spatial coverage, such as 1–4 axial slices on the ECAT (Phelps et al., 1978) or ECAT-II system (EG&G Ortec, Inc.), and up to 7 slices on the PETT VI system (Ter-Pogossian et al., 1982). In-plane spatial resolution ranged from 11.7 mm (Mintun et al., 1984) to 16 mm (Pantano et al., 1985), with slice separation between 14.4 mm (Herscovitch et al., 1985) and 19 mm (Lebrun-Grandie et al., 1983), (Pantano et al., 1985). Later scanners enabled 2D [^{15}O]-PET with extended coverage and higher spatial resolution: for instance, 35 slices with 4.6–5.7 mm in-plane resolution and 4.0–5.3 mm slice thickness on the GE ADVANCE system (GE Medical System, Milwaukee) (Okazawa et al., 2001a); or 47 slices with $5.8 \times 5.8 \times 5.0$ mm^3 resolution on the ECAT EXACT system (CTI Inc., Knoxville) (Maeda et al., 2015). These high-resolution images are smoothed during reconstruction using a Gaussian or Hanning filter with 5.5–7.0 mm full-width half maximum to improve SNR. While early PET scans corrected for attenuation using a transmission scan with an external source (^{68}Ge/^{68}Ga, ^{68}Ga/^{68}Ga, or ^{137}Cs), modern PET/CT scanners use a low-dose CT from the subject to perform attenuation correction.

A major advance in scanner hardware has been 3-dimensional (3D) acquisition of all axial lines of response without the use of collimating septa (DeGrado et al., 1994). True 3D PET provides higher sensitivity, which enables lower radiation dose or higher spatial resolution. [^{15}O]-gas PET scanned in 3D mode recently achieved 4.8-mm resolution on the Philips Gemini TF PET/CT scanner (Magota et al., 2017); 4.5-mm resolution on the GE Discovery PET/CT 710 scanner (Wagatsuma et al., 2017); and 4.3-mm intrinsic in-plane resolution on the Siemens ECAT HR þ scanner (Hattori et al., 2004). Ibaraki et al. directly compared 2D acquisition (SET-2300W scanner, Shimadzu Corp.) to 3D acquisition (SET-3000GCT/M scanner, Shimadzu Corp.) of [^{15}O]-oxygen PET on the same day in healthy volunteers (Ibaraki et al., 2008). 3D acquisition was achieved with only a quarter of the tracer dose used in 2D scans, but also greatly increased the number of scattered photons in the image. While scatter comprises only 10% of detected photons in 2D scans, the fraction of scattered

photons is much higher for 3D scans due to the presence of [^{15}O]-oxygen remaining in the gas mask, respiratory airways, and nasal passages (Ibaraki et al., 2011; Hori et al., 2014) (Fig. 2a). Standard scatter correction routines have difficulty correcting for scatter from outside the field-of-view, such as residual tracer in the gas delivery lines.

Increased scatter in 3D gas PET can lead to erroneously high values for gray-to-white matter ratio of $CMRO_2$ and requires correction. Ibaraki et al. applied a dual-energy hybrid approach (Ferreira et al., 2002) to account for scatter, based on knowledge that scattered photons have a lower energy distribution (below 480 keV) than the standard energy window (300–700 keV) for detecting PET photons. With appropriate scatter correction, gray matter $CMRO_2$ was not different for 3D acquisition (3.8 ± 0.7 ml/100 g/min) versus 2D acquisition (3.5 ± 0.5 ml/100 g/min), except focally in the pons, parahippocampus, and midbrain outside the center of the field-of-view (Ibaraki et al., 2008) (Fig. 3). Model-based correction estimates the total single scatter outside the primary emitting object, and then scales the scatter distribution tail in sinogram space (Wangerin et al., 2018). Tail-scaling methods can be combined with Monte Carlo simulation (Magota et al., 2017) to achieve scatter correction during 3D [^{15}O]-gas PET without “cold” artifacts near areas of high activity such as the gas mask.

External shields attached to the scanner or near the subject have also been tested to reduce scatter photons from large amounts of [^{15}O]-tracer in the lungs and blood pools outside the field of view. The removable external shields primarily comprise of lead (Ibaraki et al., 2011; Spinks et al., 1998; Thompson et al., 2001), although steel alloy with tungsten-impregnated rubber have also been adopted (Wagatsuma et al., 2017). For instance, Ibaraki et al. combined a 20-mm thick lead plate attached laterally to the PET detector ring (corresponding to 97% attenuation of 511-keV gamma rays) with removable 7-mm thick, lead neck-shield plates (corresponding to 70% attenuation of 511-kEv gamma rays) around the gantry bed (Ibaraki et al., 2011). Annular geometries for neck shields have also been used to improve the noise-equivalent count rate of [^{15}O]-PET images by 25% (Spinks et al., 1998) and to reduce the random counts rate by an approximate factor of 1.5 when positioned above the subject’s shoulders (Thompson et al., 2001).

3.2. Tissue heterogeneity

The achievable spatial resolution is important because tissue heterogeneity within a voxel can lead to substantial errors in OEF and $CMRO_2$ even in carefully controlled experiments (Correia et al., 1985) (Fig. 2b). For steady-state [^{15}O]-oxygen PET, OEF values are underestimated in low OEF conditions (e.g. tumors), even without considering potential CBF errors (Lammertsma and Jones, 1992). Correia et al. simulated that tissue heterogeneity is a substantial problem when gray matter comprises 20–40% of the voxel volume, in large part because of propagated error in CBF. In such voxels, if the true gray matter OEF doubles, [^{15}O]-oxygen PET will underestimate OEF by 12%; and if true gray matter OEF is halved, PET will overestimate OEF by 14% (Correia et al., 1985). Similarly, Sadato et al. also observed up to 20% error in OEF and $CMRO_2$ for voxels with low gray matter fraction (less than 25%) from independent simulations (Sadato et al., 1993). On the other hand, bolus [^{15}O]-oxygen PET provides a more linear relationship between PET counts and the

underlying physiology with less tissue heterogeneity effect, even if the shape of the input curve varies (Iida et al., 1991).

The effect of tissue heterogeneity also depends on PET scan time (Fig. 2a). Steady-state PET scans typically last 3–6 min, and a longer scan duration improves the SNR (Shidahara et al., 2008) of the acquired image and reduces quantitative bias. Shorter procedures have been simulated by sampling PET counts during the buildup and near-equilibrium phases of [^{15}O]-tracer accumulation, before the steady-state (Sadato et al., 1993). Although quantification can be achieved from "steady-state" scans acquired only 3 min after [^{15}O]-O_2 inhalation, such protocols are susceptible to error from tissue heterogeneity and to $CMRO_2$ underestimation. Furthermore, static scans cannot correct for delay and dispersion of the tracer relative to the blood input function. This correction requires dynamic acquisition, which has different sensitivity to tissue heterogeneity errors, depending on the PET detectors and SNR over time.

3.3. Arterial blood sampling

The goal of arterial blood sampling in dynamic [^{15}O]-oxygen studies is to characterize the tracer input function for kinetic modeling. Sampling is often performed manually with 0.5–5 ml of arterial blood taken from the radial or brachial artery at multiple time points after tracer administration. The sampling rate is faster immediately after tracer inhalation (e.g., every 5 s) (Mintun et al., 1984; Meyer et al., 1987), while later blood samples can be acquired with larger time intervals (e.g., every 30 s) (Ohta et al., 1992; Okazawa et al., 2001b). Radioactivity in the blood samples is measured with a scintillation detector that has been cross-calibrated with the PET scanner. Automated sampling has also been performed with infusion pumps (Kudomi et al., 2013) and detectors such as the Pico-Count radioactivity detector (Okazawa et al., 2001a) (Bio-scan, Inc., Washington D.C.); Veenstra Instruments sampler (Boellaard et al., 2001) (now Comecer Group, Netherlands); Allogg system (Alogg AB, Mariefred, Sweden); and the Twilite system (Zhang et al., 2014) (SwissTrace GmbH, Menzingen, Switzerland). Flow rates for continuous blood sampling range from 2 to 10 ml/min, and automated samples are often cross-calibrated against manual samples in the same experiment. The input function requires correction for time delay and dispersion between the peripheral arteries (from where blood is drawn) and carotid arteries that supply the brain.

For [^{15}O]-oxygen scans, the input function should also be corrected for radiolabeled metabolites. Blood samples are centrifuged to separate plasma from red blood cells, and the plasma radioactivity is assumed to only reflect recirculating metabolic [^{15}O]-water. Whole-blood and plasma radioactivity (e.g., 1.5 ml whole blood and 0.5 ml plasma) from the same time point are then measured by the well counter. By having both whole blood ([^{15}O]-oxygen plus [^{15}O]-water) and plasma ([^{15}O]-water) radioactive concentrations, the contribution of metabolic [^{15}O]-water to the input curve can be corrected, especially as it accumulates during later periods after 2 min (Fig. 1). Correction for recirculating [^{15}O]-water is more challenging for bolus inhalation experiments because continuous blood sampling and multiple measurements of [^{15}O] radioactivity are necessary during the PET scan. The calculation for bolus experiments thus often requires additional assumptions about

the temporal evolution of metabolite radioactivity. On the other hand, in steady-state [^{15}O]-oxygen experiments, this plasma correction requires only a single blood sample (Frackowiak et al., 1980) or up to three samples (Yamaguchi et al., 1986; Leenders et al., 1990) during the PET acquisition at equilibrium. As only a few blood samples are needed, the steady-state method is less labor-intensive for blood sampling and may require less medical staff than bolus inhalation. Modeling approaches have assumed a constant rate of [^{15}O]-water metabolite production in arterial blood to measure $CMRO_2$ without the need for plasma separation with a centrifuge (Iida et al., 1993). Three or four total arterial blood samples are also common for [^{15}O]-CO scans to quantify CBV (Shidahara et al., 2002; Hatazawa et al., 1995; Ibaraki et al., 2008; Hattori et al., 2004), while flow quantification for [^{15}O]-water PET usually depends on dynamic blood sampling procedures.

3.4. Kinetic modeling and parameter estimation

The final outputs of the [^{15}O]-PET procedures are quantitative, parametric maps or regional values of OEF (%) and $CMRO_2$ (ml oxygen/100 g/min). These parameters are calculated from the [^{15}O]-tracer tissue radioactivity, arterial blood input functions, and the appropriate kinetic model equations (Mintun et al., 1984; Frackowiak et al., 1980; Ohta et al., 1992; Grubb et al., 1978). Model fits in the literature have often been performed sequentially, i.e. parameters such as CBF and CBV are calculated first from separate scans and then incorporated into the OEF and $CMRO_2$ fitting procedures. Some dynamic methods also fit for the water partition coefficient between the vascular and tissue compartments during the modeling, instead of assuming a fixed value as in steady-state methods. For group analysis to compare subject cohorts or different scan techniques, parametric oxygenation maps are normalized into a brain template such as the Talaraich (Okazawa et al., 2001b) or Montreal Neurological Institute space, using structural information from a separate MRI or CT scan.

There are two approaches to calculate OEF and $CMRO_2$ using the bolus inhalation method, which correspond to slightly different compartment models. For the one-tissue model by Mintun et al. (1984) that is depicted in Fig. 1, autoradiographic (static) PET scans from [^{15}O]-oxygen and [^{15}O]-water are fed into a look-up table for image calculation. On the other hand, a different one-tissue compartment model has also been used to obtain $CMRO_2$ first. In this “one-step approach”, $CMRO_2$ is first measured directly through the equation:

$$CMRO_2 = K_1 \times (\text{arterial blood } O_2 \text{ concentration})$$

where K_1 is the tracer delivery rate. Because K_1 = OEF x CBF, in this latter method, OEF is determined after the $CMRO_2$ calculation with use of a separate CBF image. The latter one-tissue model has been implemented using weighted-integration (Ohta et al., 1992) and mathematical approaches (Kudomi et al., 2005). To calculate $CMRO_2$, the arterial blood O_2 concentration is determined from the partial pressure of oxygen (PaO_2), pH, and hematocrit values, with an assumed amount of binding of oxygen to hemoglobin molecules (Collins et al., 2015). This relationship is characterized by the oxygen dissociation curve, and in practice the arterial blood O_2 concentration is often indirectly measured through pulse oximetry.

More sophisticated parameter estimation approaches have also been adopted to quantify OEF and $CMRO_2$. Chen et al. implemented a Bayesian framework to compute $CMRO_2$ from multiple dynamic [^{15}O]-PET studies (Chen et al., 1988), which treats CBF and CBV values from separate PET scans as approximations with some level of measurement uncertainty. The Bayesian formulation incorporates prior information about the intermediate CBF and CBV parameters to improve $CMRO_2$ estimates in the presence of substantial signal noise, but may be biased in pathological conditions where the priors are inaccurate. Similarly, Ho et al. proposed a simultaneous least-squares approach that jointly analyzes dynamic [^{15}O]-oxygen and [^{15}O]-water data (Ho et al., 1998), avoiding the need to first estimate intermediate parameters (CBF and the volume of distribution). $CMRO_2$ calculated by the simultaneous least-squares method was also robust to noise, with less than 2% observed error. Holden et al. extended this concept further by estimating multiple parameters ($CMRO_2$, CBF, arterial input, blood-brain coefficient, CBV) from a single [^{15}O]-oxygen dynamic time course (Holden et al., 1988). This method performed well if the assumed relative distribution volume for water is appropriately selected, and suggests that full $CMRO_2$ mapping from a single [^{15}O]-oxygen PET scan is possible, given adequate image SNR and appropriate modeling.

3.5. Practical implementation of [^{15}O]-gas experiments

The successful administration of gas radiotracers necessitates unique safety and procedural considerations. Several radiochemistry production routes exist to generate [^{15}O]-tracers (Dick et al., 2015), which may be sampled with an oxygen gas trap for radiochemical purity assays. Once produced, the [^{15}O]-gases are regulated and shipped to the imaging scanner through systems that vary from site to site. For instance, some sites have cyclotrons that are located up to several thousand feet from the scanner, and require shielded delivery through pneumatic tubes and an inhalation controller at the scanner location. The inhalation controller is a circuit that regulates the gas tracer delivery rate and consists of components such as a mass flow controller, a radioactive detector, and a flow meter (Iguchi et al., 2018). Investigators should check for gas leaks using the flow meter and a test carrier gas before the start of each experiment. Furthermore, technologists should clarify how to quickly open or secure respiration tubing during the study to minimize radiation exposure.

At the scanner end, the tracer dose to be breathed is monitored using a radiation detector such as an ionization chamber. The chamber encloses the inhalation bag (2–3 L) that holds the tracer gas and is commonly lead-shielded. It applies an electric field to directly ionize the gas tracer and measure the tracer dose. The ionization chamber dose measurement should be accurately calibrated, which depends on the inhalation bag geometry and may be difficult to cross-calibrate with standard well counters that only hold smaller samples. Patients also should be suitably prepared for the gas tracer administration. Participants may be cued, for example, to take a deep breath at a certain time point determined by the investigator to achieve a target bolus tracer dose. The participants may be similarly prompted to exhale deeply back into the respiration bag, to measure and subtract out any residual, exhaled tracer and safely contain it. Depending on local and health physics safety requirements, the air of the entire PET room may be exhausted at a rate of up to 20 complete air changes per hour (Iguchi et al., 2018). This air flow ensures that exhaled or leaked gas tracer does not become

trapped in the scanner facility and add unnecessary radiation to the subject or to investigators. A separate gamma ray monitor can be placed outside the room exhaust duct to monitor the gaseous radioactivity carried out of the PET room.

4. Normal range and reproducibility of quantitative oxygen extraction and metabolism

4.1. Meta-analysis of OEF and $CMRO_2$ values in healthy volunteers from [^{15}O]-PET

To understand the normative range for brain oxygen usage, we performed a meta-analysis of quantitative PET studies that reported OEF and $CMRO_2$ in the gray and white matter of healthy volunteers. Fifteen [^{15}O]-oxygen PET studies that fulfilled these criteria were identified based on a PubMed search of the terms “oxygen PET” and “O-15 PET”. Random-effects meta-analysis was performed (Hedges, 1983), which assumes that the observed studies are a random sample from a larger population of studies and have (randomly) different study effect sizes. Forest plots of the mean values and effect sizes for OEF (Fig. 4) and $CMRO_2$ (Fig. 5) across individual studies were generated in Stata version 16 software (StataCorp, College Station, TX). Sub-group meta-analysis was used to separate gray and white matter values as well as bolus versus continuous inhalation methods, resulting in four sub-groups of PET studies.

OEF was not different between gray matter (mean 0.43, confidence interval CI: 0.41–0.45) and white matter (0.42, CI: 0.39–0.44) when considered across all studies (Fig. 4). The continuous inhalation method tended to measure higher OEF values by a few percent absolute oxygenation than bolus inhalation ($P = 0.01$). Variation in OEF values across studies includes both true study-to-study variation (“heterogeneity”) and random variation. For each sub-group in the meta-analysis, we calculated the I^2 statistic, which is a ratio of the estimated “true” heterogeneity among studies to the total observed variation (Higgins and Thompson, 2002). Thus, the I^2 statistic reflects the inconsistency across studies; a lower I^2 indicates more consistency across studies. Generally, each sub-group showed large heterogeneity between studies, with large I^2 values of greater than 80%, except for white matter OEF values in bolus inhalation studies, which had a moderate I^2 value of 48.7%. This heterogeneity reflects wide variation in specific imaging methods adopted by investigators, as well as different delineation of regions of interest. OEF values in our meta-analysis were concordant with the overall cortical OEF of 0.44 ± 0.06 previously reported for 11 PET centers (70 subjects) in Japan (Ito et al., 2004).

On the other hand, $CMRO_2$ was substantially higher in gray matter (4.45 ml/100 g/min, CI: 3.93–4.98) compared to white matter (1.68 ml/100 g/min, CI:1.54–1.82) (Fig. 5). Even larger heterogeneity was observed across studies, with I^2 values mostly greater than 95%, except for white matter $CMRO_2$ in bolus inhalation studies, which showed a moderate I^2 value of 69%. This higher variance may reflect the added CBF measurement uncertainty used in computing $CMRO_2$ values, individual variations in blood oxygen concentration, and variable methods across studies. A variety of correction approaches for vascular PET counts have also been adopted, which may lead to over-correction in veins for bolus inhalation scans or $CMRO_2$ overestimation in Ohta’s one-step calculation approach (Ohta et al., 1992).

Due to this large measurement heterogeneity, no difference in $CMRO_2$ values was found between continuous versus bolus inhalation techniques ($P = 0.273$). One caveat to this observation is that steady-state studies in this meta-analysis are generally older than bolus inhalation studies, such that some of the $CMRO_2$ differences may be attributed to the evolution of PET scanner technologies over multiple decades. $CMRO_2$ from bolus inhalation studies in our meta-analysis (3.8 ml/100 g/min) was more similar to the mean cortical $CMRO_2$ (3.3 ± 0.5 ml/100 g/min) reported for 11 Japanese PET centers in the literature (Ito et al., 2004).

4.2. Measurement reproducibility

The value of [^{15}O]-PET to identify pathophysiology in disease depends on the reliability of the OEF and $CMRO_2$ measurements across subjects and from session to session. In 10 healthy volunteers and 24 patients with head injury, Coles et al. characterized the inter-subject (between individuals) coefficient of variation (CoV) of oxygenation scans using steady-state 2-dimensional PET (Coles et al., 2006). The inter-subject CoV between healthy individuals was 7.3% for OEF and 12.8% for $CMRO_2$. Neurological patients, on the other hand, exhibited higher CoV of 22.5% for OEF and 23.2% for $CMRO_2$, which may reflect disease-specific differences in oxygen utilization. Part of the inter-subject CoV is driven by physiological differences, such as in hematocrit values between people (Ibaraki et al., 2010) or in intermediate parameters such as CBV of up to 15.2% in healthy volunteers and 22.5% in patients (Coles et al., 2006). Ito et al. found that within a center, [^{15}O]-PET measurements are relatively stable, showing only 0.2% within-center CoV in OEF and a moderate CoV of 18.9% in $CMRO_2$ estimates (Ito et al., 2004). However, acquisitions differ across research sites and can contribute up to 76.8% variation in $CMRO_2$ quantification between centers (Ito et al., 2004), suggesting that technique harmonization is important to adopt [^{15}O]-oxygen PET in multi-center trials.

Bremmer et al. performed test-retest [^{15}O]-PET studies in seven healthy volunteers (mean age 69 years), with scan sessions separated by 3–54 days (Bremmer et al., 2011). In the whole brain, day-to-day CoV was 9.3% for OEF and 5.3% for $CMRO_2$ as measured by a brief inhalation PET method. Some of the test-retest CoV can be attributed to underlying physiological fluctuations, including larger variation in OEF values that accompany day-to-day changes in brain perfusion. On the other hand, the day-to-day variability of $CMRO_2$ estimates was very low and may reflect healthy neurovascular coupling in control subjects to maintain stable brain oxygen metabolism during brain function (Rhodes et al., 1981). The day-to-day reproducibility of left-to-right ratios of these parameters was even more robust, with less than 1.5% CoV for OEF ratios and less than 4.0% CoV for $CMRO_2$ ratios in gray matter vascular territories (Bremmer et al., 2011). This finding suggests that left-right ratios of OEF and $CMRO_2$ will be highly useful in patients with asymmetric disease (e.g., unilateral steno-occlusion), due to their excellent test-retest repeatability.

5. Identification of hemodynamic impairment with [^{15}O]-PET in cerebrovascular disease

Quantitative [^{15}O]-oxygen PET provides critical assessment of the stages of hemodynamic failure in carotid occlusion (Grubb et al., 1998; Derdeyn et al., 1998), distinguishing of disease-driven metabolic changes from the brain's compensatory mechanisms (Derdeyn et al., 1999a), and prediction of future stroke risk based on high, abnormal OEF ("misery perfusion") (Hokari et al., 2009; Yamauchi et al., 1999) or loss of cerebrovascular reserve (Nariai et al., 1995, 1998; Gibbs et al., 1984). Longitudinal studies (Wise et al., 1983) of cerebrovascular patients have determined absolute OEF thresholds above which brain tissue is considered at-risk, based on PET imaging in a comparable healthy cohort. For instance, Yamauchi et al. identified abnormal OEF as absolute hemispheric OEF values above the upper 95% confidence limits in 10 age-matched healthy volunteers (Yamauchi et al., 1999), and Hokari et al. identified elevated OEF as values greater than 2 standard deviations above the healthy control mean (Hokari et al., 2009). Absolute OEF thresholds ranged from 0.50[86, 92] to 0.59[93], and elevated OEF independently predicted an increased 5-year risk of stroke in the hemisphere ipsilateral to the carotid artery occlusion. Fig. 6a illustrates longitudinal [^{15}O]-PET imaging in three patients with unilateral occlusive carotid artery disease. Focal areas of high absolute OEF (ranging from 0.51 to 0.58) corresponded to eventual lesion development on follow-up MRI after 9–24 months (Hokari et al., 2009).

Full OEF quantification, which requires arterial blood sampling and sophisticated image analysis, is unfortunately not always practical in clinical imaging studies. Multiple relative OEF metrics to detect hemodynamic impairment that avoid some of these challenges have been proposed as alternatives (Fig. 6b). Even when absolute quantification is possible, many studies calculated a relative OEF asymmetry index using a ratio of OEF in the ischemic to normal-appearing hemispheres (Derdeyn et al., 1998; Powers et al., 1984, 1987; Okazawa et al., 2007). OEF images are first registered to a brain template space, and detection of elevated OEF is based on the asymmetry index between the two hemispheres. This metric has been used to show the effectiveness of extra-cranial to intracranial bypass surgery to reduce OEF in the symptomatic hemisphere of patients with carotid artery occlusion (Powers et al., 1984). One advantage of the asymmetry index is that the unaffected hemisphere serves as a "control" within the same patient, and the ratio accounts for normal global OEF variations between individuals. However, the asymmetry index is less informative for patients with bilateral disease.

Use of a count-based asymmetry index (Grubb et al., 1998; Derdeyn et al., 1999b), which calculates the ratio between hemispheres directly from the observed PET counts, further simplifies OEF assessment in patients. In the count-based approach, the [^{15}O]-oxygen PET scan is divided by the [^{15}O]-water PET scan after normalizing each image to the same template space. This ratio is expected to be linear with quantitative OEF (except for small contributions from unbound oxygen tracer and recirculating water) (Grubb et al., 1998), and simplifies the image processing as kinetic models are not required. Derdeyn et al. directly compared count-based to full quantitative OEF methods to stratify patients with symptomatic carotid occlusion and monitor ischemic events throughout an average 3-year

period. Both quantitative and count-based OEF metrics were predictive of stroke during follow-up, and receiver operator curve (ROC) analysis showed that count-based OEF asymmetry showed overall higher sensitivity and specificity. Because the count-based method derives directly from the measured PET counts, its accuracy depends on the duration of the acquired scan, with longer scans showing better agreement with calculated OEF asymmetry indices (Kobayashi et al., 2008). For patients with bilateral disease, alternative reference regions such as the cerebellum have been used to normalize [^{15}O]-oxygen PET counts and are also predictive of recurrent stroke (Jiang et al., 2010). Table 2 summarizes literature using multiple OEF approaches to assess hemodynamic impairment in cerebrovascular disease, and the corresponding thresholds derived from healthy controls in the same studies.

Different clinically feasible OEF metrics have been directly compared in larger clinical imaging trials of cerebrovascular patients. The St. Louis Carotid Occlusion Study (STLCOS), for instance, recruited 81 patients with symptomatic carotid artery occlusion into a prospective trial to test whether increased OEF predicts future stroke risk (Grubb et al., 1998). Based on data from this trial, ROC analysis revealed that the count-based ratio had the highest area under the curve (AUC = 0.815) performance, followed by absolute OEF (AUC = 0.769) and the OEF ratio between hemispheres (AUC = 0.737) (Derdeyn et al., 2001). These observations were only partially consistent with previous comparisons done in a similar cohort (Yamauchi et al., 1999), and highlight that the selection of OEF threshold and consideration of bilateral disease can strongly influence patient stratification.

The Carotid Occlusion Surgery Study (COSS) (Grubb et al., 2003) subsequently enrolled patients with carotid artery stenosis and OEF impairment detected by [^{15}O]-PET, who were randomized to receive medical treatment (N = 98) or extra-to intracranial bypass surgery (N = 97). Disappointingly, the COSS trial failed to show a benefit of bypass surgery in reducing two-year stroke rate and was prematurely terminated (Powers et al., 2011). Later reanalysis (Carlson et al., 2011), however, suggested that the count-based ratio PET method used in the study may not have adequately identified patients with hemodynamic impairment who could benefit from surgery. Some of the methodological compromises in COSS, including use of relative metrics to facilitate multi-center participation and lowering the OEF threshold to increase patient enrollment, thus may have confounded the study conclusions about the surgery's efficacy in carotid artery disease (Carlson et al., 2011). These technical confounds point to the continued need for clinically feasible, accurate OEF imaging development, i.e., to select between new endovascular therapies to manage asymptomatic carotid artery disease (Marshall et al., 2018), for which treatment guidelines are outdated and mixed.

6. Advanced techniques for PET oxygenation imaging

6.1. Reducing scan time

To make OEF and $CMRO_2$ images more easily attainable, technical improvements have aimed to shorten the necessary scan time for [^{15}O]-PET. Kudomi et al. proposed a dual autoradiography approach that acquires PET images during rapid administration of two tracers, [^{15}O]-oxygen and [^{15}O]-water, in a span of 3 min (Kudomi et al., 2005). The analysis utilizes a look-up table formulation that mathematically accounts for residual

radioactivity from the first tracer and quantifies OEF, CBF, and $CMRO_2$, regardless of which of the two tracers was administered first. Combined with dynamic PET acquisition, this dual-tracer method was extended to estimate and account for blood volume, using a "single-step" $CMRO_2$ calculation and basis function reconstructions (Kudomi et al., 2013). This updated technique can only compute V_0 (the arterial-to-capillary blood volume) for vascular corrections and not the total CBV (which includes venous volume). Although the dual-tracer approach led to increased statistical noise in the estimated parameters, it provided accurate absolute OEF and $CMRO_2$ values (within 7% of reference acquisitions) in a total scan time of under 15 min.

Based on promising simulations (Huang et al., 1986), Meyer et al. implemented a nonlinear regression to estimate multiple parameters (CBF, OEF, CBV, $CMRO_2$) from a single, dynamic [^{15}O]-oxygen PET scan (Meyer et al., 1987). Although use of a single tracer markedly reduced the scan time and radiation dose, only regional $CMRO_2$ (and not the other parameters) could be reliably fit. Additionally, the quality of the $CMRO_2$ fit was only acceptable for data during the first minute after [^{15}O]-oxygen bolus inhalation, suggesting the model is valid primarily for short time frames that are subject to high statistical noise. Ohta et al. compared different kinetic models of brain physiology, for instance with different representations of recirculating [^{15}O]-water, to model a single dynamic [^{15}O]-oxygen scan (Ohta et al., 1992). Using time-weighted integration, the study measured accurate $CMRO_2$ values from the initial 3 min of dynamic [^{15}O]-oxygen uptake after inhalation. While $CMRO_2$ estimates had favorable noise properties in the normal range of oxygen consumption, the "one-step method" was sensitive to delays between the arterial input function and the brain (Ohta et al., 1992), and requires proper time shift correction for accurate analysis (Islam et al., 2017a). Beyond shorter scan times, the single-step approach offers the advantage of removing physiological drifts in CBF and CBV that occur between separate [^{15}O]-oxygen and [^{15}O]-water and [^{15}O]-CO scans.

6.2. Reducing the invasiveness of PET input functions

The technical challenge and invasiveness of arterial blood sampling limits the accessibility of quantitative [^{15}O]-PET methods. Even when blood sampling is available, peristaltic pump failures or inadequate access to peripheral arteries may result in failures (Su et al., 2017). An image-derived input function (IDIF) alternative that does not require blood sampling is thus ideal, especially as global OEF and $CMRO_2$ may vary both in healthy controls and patients. The advent of total-body PET scanners, with large axial field-of-view that includes the heart, enables IDIFs to be estimated from the aorta (Badawi et al., 2019; Zhang et al., 2020). IDIF methods for [^{15}O]-water have been proposed (Islam et al., 2017b; Okazawa et al., 2018; Boellaard et al., 2005; Khalighi et al., 2018), some benefitting from structural localization of cervical arteries on MRI angiography in the same subject. Unlike [^{15}O]-water, however, [^{15}O]-oxygen is consumed by tissues and requires advanced IDIF techniques to separate radiolabeled metabolites from the parent tracer in PET blood voxels.

Kudomi et al. developed an IDIF approach for [^{15}O]-oxygen that parameterizes the IDIF formula based on the underlying [^{15}O]-oxygen exponential kinetic model (Kudomi et al., 2018). This IDIF expression assumed a constant generation rate of recirculating water (k)

and analytical relationships with the brain tissue activity curves measured by PET. For in vivo datasets, the IDIF rate constants were jointly estimated from multiple observed tissue curves, and mean values of the rate parameters were used to generate the final IDIF for OEF and $CMRO_2$ analysis. During sequential inhalation of [^{15}O]-water and [^{15}O]-CO_2, the estimated IDIFs showed great fidelity (R^2 correlation = 0.97) to measured input functions from blood in cerebrovascular patients (Kudomi et al., 2018).

When calculating IDIFs from smaller vessels such as the carotid arteries, potential artifacts should be corrected based on vessel geometry, as visualized on co-registered MR angiograms or black-blood images (Iguchi et al., 2013). IDIFs require correction for small recovery coefficients (which lead to underestimation in larger PET voxels) depending on vessel size; and correction for spill-in artifacts from adjacent tissue (which lead to overestimation at later time points). Su et al. implemented an IDIF method for [^{15}O]-oxygen that included a recovery coefficient correction for cervical arteries (automatically segmented on MR angiogram) and a PET spatial resolution of 8 mm (Su et al., 2017). The IDIF was also parameterized based on rate constants in the kinetic model, and assumed a constant production rate of metabolic water of $k = 0.072\ \text{min}^{-1}$. The authors directly compared IDIF- and blood-based quantification of hemodynamic parameters from [^{15}O]-oxygen PET in healthy controls. Intra-class correlation between the two methods was high for CBF (ICC = 0.85) and $CMRO_2$ (ICC = 0.82), but was lower for CBV (ICC = 0.44), likely because the CBV estimate had the most noise and least physiological variation across volunteers (Su et al., 2017).

7. Comparison with MRI and opportunities with simultaneous PET/MRI

7.1. Cerebral blood volume assessment by MRI

Non-invasive MRI approaches (Hua et al., 2019) to measure CBV may enable corrections for tracer in the blood pool during [^{15}O]-oxygen PET studies, without the need for a separate [^{15}O]-CO scan. CBV imaging also provides important assessment of brain blood flow auto-regulation in its own right, and is a sensitive indicator of tissue viability in cerebrovascular disease, tumors (van Westen et al., 2011), and dementia (Mak et al., 2012). The MRI methods include dynamic susceptibility contrast (DSC) (Welker et al., 2015), which tracks a bolus of gadolinium contrast to measure relative CBF and CBV; as well as vascular space occupancy (VASO) (Lu et al., 2005), which maps relative CBV without contrast injection. VASO MRI uses a blood-nulling, non-selective inversion recovery sequence to distinguish between blood and tissue within a voxel, based on different T_1 relaxation times in the two compartments. VASO is often used to detect relative CBV changes during functional paradigms, although absolute CBV quantification is possible with contrast agent if T_2/T_2^* relaxation and acquisition effects are carefully considered (Lu et al., 2005; Uh et al., 2009).

If MRI scans of CBV are available in the same individual, the high-resolution CBV image (~1.5 mm) could take the place of the [^{15}O]-CO PET scan in kinetic modeling (Fig. 7a). Such a multi-modal approach to would benefit from simultaneous acquisition offered by hybrid PET/MRI scanners. Using a porcine model, Østergaard et al. directly compared absolute CBV values from DSC MRI (after normalization of contrast dose and CBF) to separate [^{15}O]-CO PET scans in the same animals (Ostergaard et al., 1998). Although PET

and MRI CBV values showed strong correlations, PET values were 2.5 times larger than absolute MRI values, which may reflect different sensitivity of MRI to smaller brain vessels. A later clinical study in Moyamoya disease found moderate correlations (R^2 = 0.47 to 0.58) between DSC and [^{15}O]-CO PET for relative CBV, with excellent specificity but limited sensitivity to abnormal CBV in patients (Tanaka et al., 2006). Similarly, arterial spin labeling MRI moderately correlated with [^{15}O]-water PET for arterial CBV across healthy volunteers, but MRI values were only 27% of the PET values on average (Heijtel et al., 2016). These discrepancies derive from imaging and physiological sources, and should be considered in order to combine MRI-based CBV measures with PET, with the goal of reducing the radiation and scan time of [^{15}O]-gas PET studies.

7.2. Novel MRI methods to image oxygenation

Emerging MRI techniques have also aimed to non-invasively image brain oxygenation, based on deoxyhemoglobin effects on quantitative blood oxygen level dependent (BOLD) signal (He and Yablonskiy, 2007; An and Lin, 2000), magnetic susceptibility (Wehrli et al., 2017; Fan et al., 2014; Zhang et al., 2015), and T_2 relaxation values in venous blood (Bolar et al., 2011; Lu and Ge, 2008). These nascent MRI methods are promising and show excellent inter-site robustness for global OEF measurements (Liu et al., 2016), but few have been directly compared to the PET reference standard. Simultaneous PET/MRI will facilitate head-to-head comparisons and optimization of oxygenation MRI relative to [^{15}O]-gas PET by ensuring that the same physiological state is observed by each modality. Previous meta-analysis has shown that improved CBF correspondence between PET and MRI is achieved if the scans are spaced closely together in time (Fan et al., 2016), minimizing the effect of natural fluctuations due to time of day, diet, and caffeine. Similar benefits are expected in comparing OEF by the two modalities, especially if multiple physiological states are observed, e.g. after vasodilation (Puig et al., 2019). Furthermore, global OEF MRI measurements from the superior sagittal sinus are more widespread and have been compared to each other with some success (Barhoum et al., 2015). Whole-brain OEF information from MRI could thus be used as a scaling factor (Ishii et al., 2020) for simultaneous [^{15}O]-oxygen PET/MRI studies and eliminate the need for invasive arterial blood sampling. Initial simulations suggest that global scaling of PET images with MRI-derived flow and whole-brain $CMRO_2$ measures is robust to signal variations related to recirculating water and CBV (Narciso et al., 2019). Human [^{15}O]-gas studies with hybrid PET/MRI are currently underway in the community.

Kudo et al. compared quantitative susceptibility mapping (QSM) MRI assessment of OEF with [^{15}O]-oxygen PET scans in 26 patients with unilateral cerebrovascular disease and 10 healthy controls, separated by a mean interval of 10 days (Kudo et al., 2016). The specific QSM MRI technique was performed at 3 T with spatial resolution of 0.66 × 1.6 × 2.0 mm^3. Vein susceptibility was measured to calculate OEF in venous blood relative to water, and averaged over larger volumes of interest in the brain using a sliding window computation (Fig. 7b). Significant correlation of the OEF ratio (affected to normal hemisphere) was observed between QSM-OEF and PET-OEF (R = 0.62, P < 0.001) (Kudo et al., 2016). Correspondingly, QSM-OEF had good sensitivity (63%) and specificity (89%) in identifying abnormal, elevated OEF in the patients, when compared to PET. In a separate cohort of

unilateral cerebrovascular patients, Uwano et al. found a similar correlation between QSM-OEF and PET-OEF ($R = 0.69$, $P < 0.001$), but better overall QSM performance in detecting elevated OEF in middle cerebral artery territories (sensitivity of 82% and specificity of 86%) (Uwano et al., 2017). This slight improvement was attributed to larger magnetic susceptibility effects at 7 T, so that MRI OEF values were derived from a larger number of smaller veins and with fewer partial volume errors. Nonetheless, residual bias between PET and MRI OEF was seen, and point to future MRI optimization and careful multi-modal OEF comparisons with simultaneous PET/MRI.

Given multi-modal information, advanced machine learning algorithms provide powerful strategies to synthesize high quality, accurate OEF and $CMRO_2$ maps. Despite its relative accessibility and flexibility, OEF measurement by MRI is often hindered by complex contributions of multiple physiological parameters and low deoxyhemoglobin signal, as with quantitative BOLD MRI. A recently proposed solution to these limitations is use of an artificial neural network to emulate the curve-fitting of dynamic quantitative BOLD signals and estimate OEF (Hubertus et al., 2019). This image transformation network takes the multi-echo gradient echo signals and magnetic susceptibility maps as inputs and outputs a final OEF map. The neural network provided smaller inter-subject variation in OEF that was more in line with PET literature, compared to standard quasi-Newton fitting of quantitative BOLD. However, the network training was performed purely on numerical datasets with simulated noise (Hubertus et al., 2019), which does not realistically model all acquisition and physiological features of OEF images. If paired oxygenation-sensitive MRI and [^{15}O]-gas PET signals are available, particularly from a simultaneous PET/MRI acquisition, a similar network can be trained using PET as the “gold standard” to enhance OEF performance. This model structure has already been successful in predicting PET-like CBF maps from MRI-only inputs in healthy volunteers and cerebrovascular patients, using paired [^{15}O]-PET and arterial spin labeling MRI scans from a simultaneous PET/MRI scanner (Guo et al., 2019). Given the complexity of [^{15}O]-oxygen PET, there is great potential for deep neural networks to synthesize multiple MRI inputs (both physiological and structural) to generate high-SNR, PET-like maps of OEF and $CMRO_2$ that are more widely available.

8. Conclusion

The ability to non-invasively assess oxygenation and oxygen metabolism in the brain offers critical insight into cerebrovascular disorders and early metabolic injury during cognitive aging and dementia. [^{15}O]-oxygen PET is an accepted imaging technique to measure OEF and $CMRO_2$, but technical understanding of different methods adopted in existing studies is important to accurately interpret physiological findings in health and disease across various sites. Continued optimization to accelerate and reduce the invasiveness of [^{15}O]-oxygen PET, as well as its synergy with emergent oxygenation MRI approaches on hybrid scanners, offer innovative avenues to develop robust, clinical imaging of brain OEF and $CMRO_2$.

Acknowledgements

We express appreciation to Dr. Bin Shen and Rowaid Kellow at Stanford University for informative discussion of practical aspects of [^{15}O]-gas PET and radiochemistry. The authors received support from the National Institutes of

Health (1K99NS102884 and 1R01NS082561) and GE Healthcare. The funders played no role in preparation of this manuscript.

References

Ackerman RH, Correia JA, Alpert NM, Baron JC, Gouliamos A, Grotta JC, et al., 1981 Positron imaging in ischemic stroke disease using compounds labeled with oxygen 15. Initial results of clinicophysiologic correlations. Arch. Neurol 38 (9), 537–543. [PubMed: 6791617]

Albers GW, Marks MP, Lansberg MG, 2018 Thrombectomy for stroke with selection by perfusion imaging. N. Engl. J. Med 378 (19), 1849–1850.

An H, Lin W, 2000 Quantitative measurements of cerebral blood oxygen saturation using magnetic resonance imaging. J. Cerebr. Blood Flow Metabol 20 (8), 1225–1236.

Badawi RD, Shi H, Hu P, Chen S, Xu T, Price PM, et al., 2019 First human imaging studies with the EXPLORER total-body PET scanner. J. Nucl. Med 60 (3), 299–303. [PubMed: 30733314]

Barhoum S, Rodgers ZB, Langham M, Magland JF, Li C, Wehrli FW, 2015 Comparison of MRI methods for measuring whole-brain venous oxygen saturation. Magn. Reson. Med 73 (6), 2122–2128. [PubMed: 24975122]

Baron JC, Jones T, 2012 Oxygen metabolism, oxygen extraction and positron emission tomography: historical perspective and impact on basic and clinical neuroscience. Neuroimage 61 (2), 492–504. [PubMed: 22227130]

Baron JC, Bousser MG, Rey A, Guillard A, Comar D, Castaigne P, 1981 Reversal of focal "misery-perfusion syndrome" by extra-intracranial arterial bypass in hemodynamic cerebral ischemia. A case study with 15O positron emission tomography. Stroke 12 (4), 454–459. [PubMed: 6976022]

Boellaard R, van Lingen A, van Balen SC, Hoving BG, Lammertsma AA, 2001 Characteristics of a new fully programmable blood sampling device for monitoring blood radioactivity during PET. Eur. J. Nucl. Med 28 (1), 81–89. [PubMed: 11202456]

Boellaard R, Knaapen P, Rijbroek A, Luurtsema GJ, Lammertsma AA, 2005 Evaluation of basis function and linear least squares methods for generating parametric blood flow images using 15O-water and Positron Emission Tomography. Mol. Imag. Biol 7 (4), 273–285.

Bolar DS, Rosen BR, Sorensen AG, Adalsteinsson E, 2011 QUantitative Imaging of eXtraction of oxygen and TIssue consumption (QUIXOTIC) using venular-targeted velocity-selective spin labeling. Magn. Reson. Med 66 (6), 1550–1562. [PubMed: 21674615]

Bremmer JP, van Berckel BN, Persoon S, Kappelle LJ, Lammertsma AA, Kloet R, et al., 2011 Day-to-day test-retest variability of CBF, CMRO2, and OEF measurements using dynamic 15O PET studies. Mol. Imag. Biol 13 (4), 759–768.

Carlson AP, Yonas H, Chang YF, Nemoto EM, 2011 Failure of cerebral hemodynamic selection in general or of specific positron emission tomography methodology?: carotid Occlusion Surgery Study (COSS). Stroke 42 (12), 3637–3639. [PubMed: 21960571]

Chen B, Huang SC, Hawkins RA, Phelps ME, 1988 An evaluation of Bayesian regression for estimating cerebral oxygen utilization with oxygen-15 and dynamic PET. IEEE Trans. Med. Imag 7 (4), 257–263.

Chida K, Ogasawara K, Kuroda H, Aso K, Kobayashi M, Fujiwara S, et al., 2011 Central benzodiazepine receptor binding potential and CBF images on SPECT correlate with oxygen extraction fraction images on PET in the cerebral cortex with unilateral major cerebral artery occlusive disease. J. Nucl. Med 52 (4), 511–518. [PubMed: 21421729]

Coles JP, Fryer TD, Smielewski P, Rice K, Clark JC, Pickard JD, et al., 2004 Defining ischemic burden after traumatic brain injury using 15O PET imaging of cerebral physiology. J. Cerebr. Blood Flow Metabol 24 (2), 191–201.

Coles JP, Fryer TD, Bradley PG, Nortje J, Smielewski P, Rice K, et al., 2006 Intersubject variability and reproducibility of 15O PET studies. J. Cerebr. Blood Flow Metabol 26 (1), 48–57.

Collins JA, Rudenski A, Gibson J, Howard L, O'Driscoll R, 2015 Relating oxygen partial pressure, saturation and content: the haemoglobin-oxygen dissociation curve. Breathe (Sheff) 11 (3), 194–201. [PubMed: 26632351]

Correia JA, Alpert NM, Buxton RB, Ackerman RH, 1985 Analysis of some errors in the measurement of oxygen extraction and oxygen consumption by the equilibrium inhalation method. J. Cerebr. Blood Flow Metabol 5 (4), 591–599.

DeGrado TR, Turkington TG, Williams JJ, Stearns CW, Hoffman JM, Coleman RE, 1994 Performance characteristics of a whole-body PET scanner. J. Nucl. Med 35 (8), 1398–1406. [PubMed: 8046501]

Derdeyn CP, Powers WJ, Grubb RL Jr., 1998 Hemodynamic effects of middle cerebral artery stenosis and occlusion. AJNR Am J Neuroradiol 19 (8), 1463–1469. [PubMed: 9763379]

Derdeyn CP, Videen TO, Fritsch SM, Carpenter DA, Grubb RL Jr., Powers WJ, 1999 Compensatory mechanisms for chronic cerebral hypoperfusion in patients with carotid occlusion. Stroke 30 (5), 1019–1024. [PubMed: 10229738]

Derdeyn CP, Videen TO, Simmons NR, Yundt KD, Fritsch SM, Grubb RL Jr., et al., 1999 Count-based PET method for predicting ischemic stroke in patients with symptomatic carotid arterial occlusion. Radiology 212 (2), 499–506. [PubMed: 10429709]

Derdeyn CP, Videen TO, Grubb RL Jr., Powers WJ, 2001 Comparison of PET oxygen extraction fraction methods for the prediction of stroke risk. J. Nucl. Med 42 (8), 1195–1197. [PubMed: 11483680]

Dick DW, Watkins GL, 2015 Synthesis of oxygen-15 water ([15O] H2O) In: Scott PJH (Ed.), Further Radiopharmaceuticals for Positron Emission Tomography and New Strategies for Their Production, vol. 2 John Wiley & Sons, Inc., Hoboken, New Jersey, pp. 105–113.

Fan AP, Bilgic B, Gagnon L, Witzel T, Bhat H, Rosen BR, et al., 2014 Quantitative oxygenation venography from MRI phase. Magn. Reson. Med 72 (1), 149–159. [PubMed: 24006229]

Fan AP, Jahanian H, Holdsworth SJ, Zaharchuk G, 2016 Comparison of cerebral blood flow measurement with [15O]-water positron emission tomography and arterial spin labeling magnetic resonance imaging: a systematic review. J. Cerebr. Blood Flow Metabol 36 (5), 842–861.

Ferreira NC, Trebossen R, Lartizien C, Brulon V, Merceron P, Bendriem B, 2002 A hybrid scatter correction for 3D PET based on an estimation of the distribution of unscattered coincidences: implementation on the ECAT EXACT HR+. Phys. Med. Biol 47 (9), 1555–1571. [PubMed: 12043820]

Fox PT, Raichle ME, 1986 Focal physiological uncoupling of cerebral blood flow and oxidative metabolism during somatosensory stimulation in human subjects. Proc. Natl. Acad. Sci. U. S. A 83 (4), 1140–1144. [PubMed: 3485282]

Frackowiak RS, Lenzi GL, Jones T, Heather JD, 1980 Quantitative measurement of regional cerebral blood flow and oxygen metabolism in man using 15O and positron emission tomography: theory, procedure, and normal values. J. Comput. Assist. Tomogr 4 (6), 727–736. [PubMed: 6971299]

Gallagher D, Belmonte D, Deurenberg P, Wang Z, Krasnow N, Pi-Sunyer FX, et al., 1998 Organ-tissue mass measurement allows modeling of REE and metabolically active tissue mass. Am. J. Physiol 275 (2), E249–E258. [PubMed: 9688626]

Gibbs JM, Leenders KL, Wise RJ, Jones T, 1984 Evaluation of cerebral perfusion reserve in patients with carotid-artery occlusion. Lancet 1 (8370), 182–186. [PubMed: 6141333]

Grubb RL Jr., Raichle ME, Higgins CS, Eichling JO, 1978 Measurement of regional cerebral blood volume by emission tomography. Ann. Neurol 4 (4), 322–328. [PubMed: 727738]

Grubb RL Jr., Derdeyn CP, Fritsch SM, Carpenter DA, Yundt KD, Videen TO, et al., 1998 Importance of hemodynamic factors in the prognosis of symptomatic carotid occlusion. J. Am. Med. Assoc 280 (12), 1055–1060.

Grubb RL Jr., Powers WJ, Derdeyn CP, Adams HP Jr., Clarke WR, 2003 The carotid occlusion surgery study. Neurosurg. Focus 14 (3), e9.

Guo J, Gong E, Fan AP, Goubran M, Khalighi MM, Zaharchuk G, 2019 Predicting (15)O-Water PET cerebral blood flow maps from multi-contrast MRI using a deep convolutional neural network with evaluation of training cohort bias. J. Cerebr. Blood Flow Metabol 10.1177/0271678X19888123.

Hatazawa J, Fujita H, Kanno I, Satoh T, Iida H, Miura S, et al., 1995 Regional cerebral blood flow, blood volume, oxygen extraction fraction, and oxygen utilization rate in normal volunteers measured by the autoradiographic technique and the single breath inhalation method. Ann. Nucl. Med 9 (1), 15–21. [PubMed: 7779525]

Hattori N, Bergsneider M, Wu HM, Glenn TC, Vespa PM, Hovda DA, et al., 2004 Accuracy of a method using short inhalation of (15)O-O(2) for measuring cerebral oxygen extraction fraction with PET in healthy humans. J. Nucl. Med 45 (5), 765–770. [PubMed: 15136624]

He X, Yablonskiy DA, 2007 Quantitative BOLD: mapping of human cerebral deoxygenated blood volume and oxygen extraction fraction: default state. Magn. Reson. Med 57 (1), 115–126. [PubMed: 17191227]

Hedges LV, 1983 A random effects model for effect sizes. Psychol. Bull 93 (2), 388–395.

Heijtel DF, Petersen ET, Mutsaerts HJ, Bakker E, Schober P, Stevens MF, et al., 2016 Quantitative agreement between [(15)O]H2O PET and model free QUASAR MRI-derived cerebral blood flow and arterial blood volume. NMR Biomed 29 (4), 519–526. [PubMed: 26876426]

Herscovitch P, Mintun MA, Raichle ME, 1985 Brain oxygen utilization measured with oxygen-15 radiotracers and positron emission tomography: generation of metabolic images. J. Nucl. Med 26 (4), 416–417. [PubMed: 3872355]

Higgins JP, Thompson SG, 2002 Quantifying heterogeneity in a meta-analysis. Stat. Med 21 (11), 1539–1558. [PubMed: 12111919]

Ho D, Feng D, Chen K, 1998 New method for the analysis of multiple positron emission tomography dynamic datasets: an example applied to the estimation of the cerebral metabolic rate of oxygen. Med. Biol. Eng. Comput 36 (1), 83–90. [PubMed: 9614753]

Hokari M, Kuroda S, Shiga T, Nakayama N, Tamaki N, Iwasaki Y, 2008 Combination of a mean transit time measurement with an acetazolamide test increases predictive power to identify elevated oxygen extraction fraction in occlusive carotid artery diseases. J. Nucl. Med 49 (12), 1922–1927. [PubMed: 18997043]

Hokari M, Kuroda S, Shiga T, Nakayama N, Tamaki N, Iwasaki Y, 2009 Impact of oxygen extraction fraction on long-term prognosis in patients with reduced blood flow and vasoreactivity because of occlusive carotid artery disease. Surg. Neurol 71 (5), 532–538 discussion 538, 538–9. [PubMed: 18514278]

Holden JE, Eriksson L, Roland PE, Stone-Elander S, Widen L, Kesselberg M, 1988 Direct comparison of single-scan autoradiographic with multiple-scan least-squares fitting approaches to PET CMRO2 estimation. J. Cerebr. Blood Flow Metabol 8 (5), 671–680.

Hori Y, Hirano Y, Koshino K, Moriguchi T, Iguchi S, Yamamoto A, et al., 2014 Validity of using a 3-dimensional PET scanner during inhalation of 15O-labeled oxygen for quantitative assessment of regional metabolic rate of oxygen in man. Phys. Med. Biol 59 (18), 5593–5609. [PubMed: 25179552]

Hua J, Liu P, Kim T, Donahue M, Rane S, Chen JJ, et al., 2019 MRI techniques to measure arterial and venous cerebral blood volume. Neuroimage 187, 17–31. [PubMed: 29458187]

Huang SC, Feng DG, Phelps ME, 1986 Model dependency and estimation reliability in measurement of cerebral oxygen utilization rate with oxygen-15 and dynamic positron emission tomography. J. Cerebr. Blood Flow Metabol 6 (1), 105–119.

Hubertus S, Thomas S, Cho J, Zhang S, Wang Y, Schad LR, 2019 Using an artificial neural network for fast mapping of the oxygen extraction fraction with combined QSM and quantitative BOLD. Magn. Reson. Med 82 (6), 2199–2211. [PubMed: 31273828]

Ibaraki M, Shimosegawa E, Miura S, Takahashi K, Ito H, Kanno I, et al., 2004 PET measurements of CBF, OEF, and CMRO2 without arterial sampling in hyperacute ischemic stroke: method and error analysis. Ann. Nucl. Med 18 (1), 35–44. [PubMed: 15072182]

Ibaraki M, Miura S, Shimosegawa E, Sugawara S, Mizuta T, Ishikawa A, et al., 2008 Quantification of cerebral blood flow and oxygen metabolism with 3-dimensional PET and 15O: validation by comparison with 2-dimensional PET. J. Nucl. Med 49 (1), 50–59. [PubMed: 18077532]

Ibaraki M, Shinohara Y, Nakamura K, Miura S, Kinoshita F, Kinoshita T, 2010 Interindividual variations of cerebral blood flow, oxygen delivery, and metabolism in relation to hemoglobin concentration measured by positron emission tomography in humans. J. Cerebr. Blood Flow Metabol 30 (7), 1296–1305.

Ibaraki M, Sugawara S, Nakamura K, Kinoshita F, Kinoshita T, 2011 The effect of activity outside the field-of-view on image signal-to-noise ratio for 3D PET with (15) O. Phys. Med. Biol 56 (10), 3061–3072. [PubMed: 21508441]

Iguchi S, Hori Y, Moriguchi T, Morita N, Yamamoto A, Koshino K, et al., 2013 Verification of a semi-automated MRI-guided technique for non-invasive determination of the arterial input function in O-15-labeled gaseous PET. Nucl. Instrum. Methods A 702, 111–113.

Iguchi S, Moriguchi T, Yamazaki M, Hori Y, Koshino K, Toyoda K, et al., 2018 System evaluation of automated production and inhalation of (15)O-labeled gaseous radiopharmaceuticals for the rapid (15)O-oxygen PET examinations. EJNMMI Phys 5 (1), 37. [PubMed: 30569426]

Iida H, Kanno I, Miura S, 1991 Rapid measurement of cerebral blood flow with positron emission tomography. Ciba Found. Symp 163, 23–37 discussion 37–42. [PubMed: 1815893]

Iida H, Jones T, Miura S, 1993 Modeling approach to eliminate the need to separate arterial plasma in oxygen-15 inhalation positron emission tomography. J. Nucl. Med 34 (8), 1333–1340. [PubMed: 8326395]

Ishii K, Kitagaki H, Kono M, Mori E, 1996 Decreased medial temporal oxygen metabolism in Alzheimer's disease shown by PET. J. Nucl. Med 37 (7), 1159–1165. [PubMed: 8965188]

Ishii Y, Thamm T, Guo J, Khalighi MM, Wardak M, Holley D, et al., 2020 Simultaneous phase-contrast MRI and PET for noninvasive quantification of cerebral blood flow and reactivity in healthy subjects and patients with cerebrovascular disease. J. Magn. Reson. Imag 51 (1), 183–194.

Islam MM, Tsujikawa T, Mori T, Kiyono Y, Okazawa H, 2017 Pixel-by-pixel precise delay correction for measurement of cerebral hemodynamic parameters in H2(15)O PET study. Ann. Nucl. Med 31 (4), 283–294. [PubMed: 28243845]

Islam MM, Tsujikawa T, Mori T, Kiyono Y, Okazawa H, 2017 Estimation of arterial input by a noninvasive image derived method in brain H2(15)O PET study: confirmation of arterial location using MR angiography. Phys. Med. Biol 62 (11), 4514–4524. [PubMed: 28480872]

Ito H, Kanno I, Kato C, Sasaki T, Ishii K, Ouchi Y, et al., 2004 Database of normal human cerebral blood flow, cerebral blood volume, cerebral oxygen extraction fraction and cerebral metabolic rate of oxygen measured by positron emission tomography with 15O-labelled carbon dioxide or water, carbon monoxide and oxygen: a multicentre study in Japan. Eur. J. Nucl. Med. Mol. Imag 31 (5), 635–643.

Jiang TT, Videen TO, Grubb RL Jr., Powers WJ, Derdeyn CP, 2010 Cerebellum as the normal reference for the detection of increased cerebral oxygen extraction. J. Cerebr. Blood Flow Metabol 30 (10), 1767–1776.

Kaisti KK, Langsjo JW, Aalto S, Oikonen V, Sipila H, Teras M, et al., 2003 Effects of sevoflurane, propofol, and adjunct nitrous oxide on regional cerebral blood flow, oxygen consumption, and blood volume in humans. Anesthesiology 99 (3), 603–613. [PubMed: 12960544]

Khalighi MM, Deller TW, Fan AP, Gulaka PK, Shen B, Singh P, et al., 2018 Image-derived input function estimation on a TOF-enabled PET/MR for cerebral blood flow mapping. J. Cerebr. Blood Flow Metabol 38 (1), 126–135.

Kobayashi M, Kudo T, Tsujikawa T, Isozaki M, Arai Y, Fujibayashi Y, et al., 2008 Shorter examination method for the diagnosis of misery perfusion with count-based oxygen extraction fraction elevation in 15O-Gas PET. J. Nucl. Med 49 (2), 242–246. [PubMed: 18199611]

Kudo K, Liu T, Murakami T, Goodwin J, Uwano I, Yamashita F, et al., 2016 Oxygen extraction fraction measurement using quantitative susceptibility mapping: comparison with positron emission tomography. J. Cerebr. Blood Flow Metabol 36 (8), 1424–1433.

Kudomi N, Hayashi T, Teramoto N, Watabe H, Kawachi N, Ohta Y, et al., 2005 Rapid quantitative measurement of CMRO(2) and CBF by dual administration of (15) O-labeled oxygen and water during a single PET scan-a validation study and error analysis in anesthetized monkeys. J. Cerebr. Blood Flow Metabol 25 (9), 1209–1224.

Kudomi N, Hirano Y, Koshino K, Hayashi T, Watabe H, Fukushima K, et al., 2013 Rapid quantitative CBF and CMRO(2) measurements from a single PET scan with sequential administration of dual (15)O-labeled tracers. J. Cerebr. Blood Flow Metabol 33 (3), 440–448.

Kudomi N, Maeda Y, Yamamoto H, Yamamoto Y, Hatakeyama T, Nishiyama Y, 2018 Reconstruction of input functions from a dynamic PET image with sequential administration of (15)O2 and [Formula: see text] for noninvasive and ultra-rapid measurement of CBF, OEF, and CMRO2. J. Cerebr. Blood Flow Metabol 38 (5), 780–792.

Lammertsma AA, Jones T, 1983 Correction for the presence of intravascular oxygen-15 in the steady-state technique for measuring regional oxygen extraction ratio in the brain: 1. Description of the method. J. Cerebr. Blood Flow Metabol 3 (4), 416–424.

Lammertsma AA, Jones T, 1992 Low oxygen extraction fraction in tumours measured with the oxygen-15 steady state technique: effect of tissue heterogeneity. Br. J. Radiol 65 (776), 697–700. [PubMed: 1393397]

Lammertsma AA, Wise RJ, Cox TC, Thomas DG, Jones T, 1985 Measurement of blood flow, oxygen utilisation, oxygen extraction ratio, and fractional blood volume in human brain tumours and surrounding oedematous tissue. Br. J. Radiol 58 (692), 725–734. [PubMed: 3879853]

Lammertsma AA, Baron JC, Jones T, 1987 Correction for intravascular activity in the oxygen-15 steady-state technique is independent of the regional hematocrit. J. Cerebr. Blood Flow Metabol 7 (3), 372–374.

Lammertsma AA, Correia JA, Jones T, 1988 Stability of arterial concentrations during continuous inhalation of C15O2 and 15O2 and the effects on computed values of CBF and CMRO2. J. Cerebr. Blood Flow Metabol 8 (3), 411–417.

Lebrun-Grandie P, Baron JC, Soussaline F, Loch'h C, Sastre J, Bousser MG, 1983 Coupling between regional blood flow and oxygen utilization in the normal human brain. A study with positron tomography and oxygen 15. Arch. Neurol 40 (4), 230–236. [PubMed: 6600924]

Leenders KL, Perani D, Lammertsma AA, Heather JD, Buckingham P, Healy MJ, et al., 1990 Cerebral blood flow, blood volume and oxygen utilization. Normal values and effect of age. Brain 113 (Pt 1), 27–47. [PubMed: 2302536]

Lenzi GL, Frackowiak RS, Jones T, Heather JD, Lammertsma AA, Rhodes CG, et al., 1981 CMRO2 and CBF by the oxygen-15 inhalation technique. Results in normal volunteers and cerebrovascular patients. Eur. Neurol 20 (3), 285–290. [PubMed: 6973469]

Liu P, Dimitrov I, Andrews T, Crane DE, Dariotis JK, Desmond J, et al., 2016 Multisite evaluations of a T2 -relaxation-under-spin-tagging (TRUST) MRI technique to measure brain oxygenation. Magn. Reson. Med 75 (2), 680–687. [PubMed: 25845468]

Lu H, Ge Y, 2008 Quantitative evaluation of oxygenation in venous vessels using T2-Relaxation-Under-Spin-Tagging MRI. Magn. Reson. Med 60 (2), 357–363. [PubMed: 18666116]

Lu H, Law M, Johnson G, Ge Y, van Zijl PC, Helpern JA, 2005 Novel approach to the measurement of absolute cerebral blood volume using vascular-space-occupancy magnetic resonance imaging. Magn. Reson. Med 54 (6), 1403–1411. [PubMed: 16254955]

Maeda Y, Kudomi N, Sasakawa Y, Monden T, Kato K, Yamamoto Y, et al., 2015 Applicability of emission-based attenuation map for rapid CBF, OEF, and CMRO2 measurements using gaseous (15)O-labeled compounds. EJNMMI Phys 2 (1), 12. [PubMed: 26501813]

Magistretti PJ, Pellerin L, 1996 Cellular mechanisms of brain energy metabolism. Relevance to functional brain imaging and to neurodegenerative disorders. Ann. N. Y. Acad. Sci 777, 380–387. [PubMed: 8624117]

Magota K, Shiga T, Asano Y, Shinyama D, Ye J, Perkins AE, et al., 2017 Scatter correction with combined single-scatter simulation and Monte Carlo simulation scaling improved the visual artifacts and quantification in 3-dimensional brain PET/CT imaging with (15)O-gas inhalation. J. Nucl. Med 58 (12), 2020–2025. [PubMed: 28646012]

Mak HK, Chan Q, Zhang Z, Petersen ET, Qiu D, Zhang L, et al., 2012 Quantitative assessment of cerebral hemodynamic parameters by QUASAR arterial spin labeling in Alzheimer's disease and cognitively normal Elderly adults at 3-tesla. J Alzheimers Dis 31 (1), 33–44. [PubMed: 22504315]

Marchal G, Benali K, Iglesias S, Viader F, Derlon JM, Baron JC, 1999 Voxel-based mapping of irreversible ischaemic damage with PET in acute stroke. Brain 122 (Pt 12), 2387–2400. [PubMed: 10581231]

Marshall RS, Lazar RM, Liebeskind DS, Connolly ES, Howard G, Lal BK, et al., 2018 Carotid revascularization and medical management for asymptomatic carotid stenosis - hemodynamics (CREST-H): study design and rationale. Int. J. Stroke 13 (9), 985–991. [PubMed: 30132751]

Menon BK, Campbell BC, Levi C, Goyal M, 2015 Role of imaging in current acute ischemic stroke workflow for endovascular therapy. Stroke 46 (6), 1453–1461. [PubMed: 25944319]

Meyer E, Tyler JL, Thompson CJ, Redies C, Diksic M, Hakim AM, 1987 Estimation of cerebral oxygen utilization rate by single-bolus 15O2 inhalation and dynamic positron emission tomography. J. Cerebr. Blood Flow Metabol 7 (4), 403–414.

Mintun MA, Raichle ME, Martin WR, Herscovitch P, 1984 Brain oxygen utilization measured with O-15 radiotracers and positron emission tomography. J. Nucl. Med 25 (2), 177–187. [PubMed: 6610032]

Mintun MA, Lundstrom BN, Snyder AZ, Vlassenko AG, Shulman GL, Raichle ME, 2001 Blood flow and oxygen delivery to human brain during functional activity: theoretical modeling and experimental data. Proc. Natl. Acad. Sci. U. S. A 98 (12), 6859–6864. [PubMed: 11381119]

Mintun MA, Vlassenko AG, Shulman GL, Snyder AZ, 2002 Time-related increase of oxygen utilization in continuously activated human visual cortex. Neuroimage 16 (2), 531–537. [PubMed: 12030835]

Narciso L, Ssali T, Anazodo U, Iida H, St Lawrence K, 2019 Initial assessment of a reference-based non-invasive hybrid PET/MRI method for imaging CMRO2. J. Cerebr. Blood Flow Metabol 39, 572–573.

Nariai T, Suzuki R, Hirakawa K, Maehara T, Ishii K, Senda M, 1995 Vascular reserve in chronic cerebral ischemia measured by the acetazolamide challenge test: comparison with positron emission tomography. AJNR Am J Neuroradiol 16 (3), 563–570. [PubMed: 7793382]

Nariai T, Senda M, Ishii K, Wakabayashi S, Yokota T, Toyama H, et al., 1998 Posthyperventilatory steal response in chronic cerebral hemodynamic stress: a positron emission tomography study. Stroke 29 (7), 1281–1292. [PubMed: 9660374]

Ogawa T, Uemura K, Shishido F, Yamaguchi T, Murakami M, Inugami A, et al., 1988 Changes of cerebral blood flow, and oxygen and glucose metabolism following radiochemotherapy of gliomas: a PET study. J. Comput. Assist. Tomogr 12 (2), 290–297. [PubMed: 3258321]

Ohta S, Meyer E, Thompson CJ, Gjedde A, 1992 Oxygen consumption of the living human brain measured after a single inhalation of positron emitting oxygen. J. Cerebr. Blood Flow Metabol 12 (2), 179–192.

Okazawa H, Kudo T, 2009 Clinical impact of hemodynamic parameter measurement for cerebrovascular disease using positron emission tomography and (15)O-labeled tracers. Ann. Nucl. Med 23 (3), 217–227. [PubMed: 19353235]

Okazawa H, Yonekura Y, Fujibayashi Y, Yamauchi H, Ishizu K, Nishizawa S, et al., 1996 Measurement of regional cerebral plasma pool and hematocrit with copper-62-labeled HSA-DTS. J. Nucl. Med 37 (7), 1080–1085. [PubMed: 8965173]

Okazawa H, Yamauchi H, Sugimoto K, Toyoda H, Kishibe Y, Takahashi M, 2001 Effects of acetazolamide on cerebral blood flow, blood volume, and oxygen metabolism: a positron emission tomography study with healthy volunteers. J. Cerebr. Blood Flow Metabol 21 (12), 1472–1479.

Okazawa H, Yamauchi H, Sugimoto K, Takahashi M, Toyoda H, Kishibe Y, et al., 2001 Quantitative comparison of the bolus and steady-state methods for measurement of cerebral perfusion and oxygen metabolism: positron emission tomography study using 15O-gas and water. J. Cerebr. Blood Flow Metabol 21 (7), 793–803.

Okazawa H, Tsuchida T, Kobayashi M, Arai Y, Pagani M, Isozaki M, et al., 2007 Can the detection of misery perfusion in chronic cerebrovascular disease be based on reductions in baseline CBF and vasoreactivity? Eur. J. Nucl. Med. Mol. Imag 34 (1), 121–129.

Okazawa H, Higashino Y, Tsujikawa T, Arishima H, Mori T, Kiyono Y, et al., 2018 Noninvasive method for measurement of cerebral blood flow using O-15 water PET/MRI with ASL correlation. Eur. J. Radiol 105, 102–109. [PubMed: 30017265]

Ostergaard L, Smith DF, Vestergaard-Poulsen P, Hansen SB, Gee AD, Gjedde A, et al., 1998 Absolute cerebral blood flow and blood volume measured by magnetic resonance imaging bolus tracking: comparison with positron emission tomography values. J. Cerebr. Blood Flow Metabol 18 (4), 425–432.

Pantano P, Baron JC, Crouzel C, Collard P, Sirou P, Samson Y, 1985 The 15O continuous-inhalation method: correction for intravascular signal using C15O. Eur. J. Nucl. Med 10 (9–10), 387–391.

Phelps ME, Hoffman EJ, Huang SC, Kuhl DE, 1978 ECAT: a new computerized tomographic imaging system for positron-emitting radiopharmaceuticals. J. Nucl. Med 19 (6), 635–647. [PubMed: 660276]

Phelps ME, Huang SC, Hoffman EJ, Kuhl DE, 1979 Validation of tomographic measurement of cerebral blood volume with C-11-labeled carboxyhemoglobin. J. Nucl. Med 20 (4), 328–334. [PubMed: 119833]

Powers WJ, Martin WR, Herscovitch P, Raichle ME, Grubb RL Jr., 1984 Extracranial-intracranial bypass surgery: hemodynamic and metabolic effects. Neurology 34 (9), 1168–1174. [PubMed: 6611520]

Powers WJ, Press GA, Grubb RL Jr., Gado M, Raichle ME, 1987 The effect of hemodynamically significant carotid artery disease on the hemodynamic status of the cerebral circulation. Ann. Intern. Med 106 (1), 27–34. [PubMed: 3491558]

Powers WJ, Clarke WR, Grubb RL Jr., Videen TO, Adams HP Jr., Derdeyn CP, et al., 2011 Extracranial-intracranial bypass surgery for stroke prevention in hemodynamic cerebral ischemia: the Carotid Occlusion Surgery Study randomized trial. J. Am. Med. Assoc 306 (18), 1983–1992.

Puig O, Henriksen OM, Vestergaard MB, Hansen AE, Andersen FL, Ladefoged CN, et al., 2019 Comparison of simultaneous arterial spin labeling MRI and (15)O-H2O PET measurements of regional cerebral blood flow in rest and altered perfusion states. J. Cerebr. Blood Flow Metabol 10.1177/0271678X19874643.

Rhodes CG, Lenzi GL, Frackowiak RS, Jones T, Pozzilli C, 1981 Measurement of CBF and CMRO2 using the continuous inhalation of C15O2 and 15O. Experimental validation using CO2 reactivity in the anaesthetised dog. J. Neurol. Sci 50 (3), 381–389. [PubMed: 6790677]

Sadato N, Yonekura Y, Senda M, Iwasaki Y, Matoba N, Tamaki N, et al., 1993 PET and the autoradiographic method with continuous inhalation of oxygen-15-gas: theoretical analysis and comparison with conventional steady-state methods. J. Nucl. Med 34 (10), 1672–1680. [PubMed: 8410280]

Senda M, Buxton RB, Alpert NM, Correia JA, Mackay BC, Weise SB, et al., 1988 The 15O steady-state method: correction for variation in arterial concentration. J. Cerebr. Blood Flow Metabol 8 (5), 681–690.

Shidahara M, Watabe H, Kim KM, Oka H, Sago M, Hayashi T, et al., 2002 Evaluation of a commercial PET tomograph-based system for the quantitative assessment of rCBF, rOEF and rCMRO2 by using sequential administration of 15O-labeled compounds. Ann. Nucl. Med 16 (5), 317–327. [PubMed: 12230091]

Shidahara M, Watabe H, Kim KM, Kudomi N, Ito H, Iida H, 2008 Optimal scan time of oxygen-15-labeled gas inhalation autoradiographic method for measurement of cerebral oxygen extraction fraction and cerebral oxygen metabolic rate. Ann. Nucl. Med 22 (8), 667–675. [PubMed: 18982469]

Spinks TJ, Miller MP, Bailey DL, Bloomfield PM, Livieratos L, Jones T, 1998 The effect of activity outside the direct field of view in a 3D-only whole-body positron tomograph. Phys. Med. Biol 43 (4), 895–904. [PubMed: 9572513]

Su Y, Vlassenko AG, Couture LE, Benzinger TL, Snyder AZ, Derdeyn CP, et al., 2017 Quantitative hemodynamic PET imaging using image-derived arterial input function and a PET/MR hybrid scanner. J. Cerebr. Blood Flow Metabol 37 (4), 1435–1446.

Subramanyam R, Alpert NM, Hoop B Jr., Brownell GL, Taveras JM, 1978 A model for regional cerebral oxygen distribution during continuous inhalation of 15O2, C15O, and C15O2. J. Nucl. Med 19 (1), 48–53. [PubMed: 621563]

Tanaka Y, Nariai T, Nagaoka T, Akimoto H, Ishiwata K, Ishii K, et al., 2006 Quantitative evaluation of cerebral hemodynamics in patients with moyamoya disease by dynamic susceptibility contrast magnetic resonance imaging–comparison with positron emission tomography. J. Cerebr. Blood Flow Metabol 26 (2), 291–300.

Ter-Pogossian MM, Ficke DC, Sr Hood JT, Yamamoto M, Mullani NA, 1982 PETT VI: a positron emission tomograph utilizing cesium fluoride scintillation detectors. J. Comput. Assist. Tomogr 6 (1), 125–133. [PubMed: 6978352]

Thompson CJ, Kecani S, Boelen S, 2001 Evaluation of a neck shield for use during neurological studies with a whole-body PET scanner. IEEE Trans. Nucl. Sci 48 (4), 1512–1517.

Uh J, Lewis-Amezcua K, Varghese R, Lu H, 2009 On the measurement of absolute cerebral blood volume (CBV) using vascular-space-occupancy (VASO) MRI. Magn. Reson. Med 61 (3), 659–667. [PubMed: 19097238]

Uwano I, Kudo K, Sato R, Ogasawara K, Kameda H, Nomura JI, et al., 2017 Noninvasive assessment of oxygen extraction fraction in chronic ischemia using quantitative susceptibility mapping at 7 tesla. Stroke 48 (8), 2136–2141. [PubMed: 28663515]

van Westen D, Petersen ET, Wirestam R, Siemund R, Bloch KM, Stahlberg F, et al., 2011 Correlation between arterial blood volume obtained by arterial spin labelling and cerebral blood volume in intracranial tumours. Magma 24 (4), 211–223. [PubMed: 21594585]

Vespa P, Bergsneider M, Hattori N, Wu HM, Huang SC, Martin NA, et al., 2005 Metabolic crisis without brain ischemia is common after traumatic brain injury: a combined microdialysis and positron emission tomography study. J. Cerebr. Blood Flow Metabol 25 (6), 763–774.

Wagatsuma K, Oda K, Miwa K, Inaji M, Sakata M, Toyohara J, et al., 2017 Effects of a novel tungsten-impregnated rubber neck shield on the quality of cerebral images acquired using (15)O-labeled gas. Radiol Phys Technol 10 (4), 422–430. [PubMed: 28823084]

Wangerin KA, Baratto L, Khalighi MM, Hope TA, Gulaka PK, Deller TW, et al., 2018 Clinical evaluation of (68)Ga-PSMA-II and (68)Ga-RM2 PET images reconstructed with an improved scatter correction algorithm. AJR Am. J. Roentgenol 211 (3), 655–660. [PubMed: 29873506]

Wehrli FW, Fan AP, Rodgers ZB, Englund EK, Langham MC, 2017 Susceptibility-based time-resolved whole-organ and regional tissue oximetry. NMR Biomed 30 (4).

Welker K, Boxerman J, Kalnin A, Kaufmann T, Shiroishi M, Wintermark M, et al., 2015 ASFNR recommendations for clinical performance of MR dynamic susceptibility contrast perfusion imaging of the brain. AJNR Am J Neuroradiol 36 (6), E41–E51. [PubMed: 25907520]

Wiedeman MP, 1963 Dimensions of blood vessels from distributing artery to collecting vein. Circ. Res 12, 375–378. [PubMed: 14000509]

Wise RJ, Bernardi S, Frackowiak RS, Legg NJ, Jones T, 1983 Serial observations on the pathophysiology of acute stroke. The transition from ischaemia to infarction as reflected in regional oxygen extraction. Brain 106 (Pt 1), 197–222. [PubMed: 6600956]

Yamaguchi T, Kanno I, Uemura K, Shishido F, Inugami A, Ogawa T, et al., 1986 Reduction in regional cerebral metabolic rate of oxygen during human aging. Stroke 17 (6), 1220–1228. [PubMed: 3492786]

Yamauchi H, Fukuyama H, Nagahama Y, Nabatame H, Ueno M, Nishizawa S, et al., 1999 Significance of increased oxygen extraction fraction in five-year prognosis of major cerebral arterial occlusive diseases. J. Nucl. Med 40 (12), 1992–1998. [PubMed: 10616876]

Zeisig V, Patt M, Becker G, Boltze J, Sabri O, Barthel H, 2014 Cerebral blood flow measurement with oxygen-15 water positron emission tomography In: Dierckx RAJO, Otte A, de Vries EFJ, van Waarde A, Luiten PGM (Eds.), PET and SPECT of Neurobiological Systems Springer, Berlin, Heidelberg, pp. 103–124.

Zhang K, Herzog H, Mauler J, Filss C, Okell TW, Kops ER, et al., 2014 Comparison of cerebral blood flow acquired by simultaneous [15O]water positron emission tomography and arterial spin labeling magnetic resonance imaging. J. Cerebr. Blood Flow Metabol 34 (8), 1373–1380.

Zhang J, Liu T, Gupta A, Spincemaille P, Nguyen TD, Wang Y, 2015 Quantitative mapping of cerebral metabolic rate of oxygen (CMRO2) using quantitative susceptibility mapping (QSM). Magn. Reson. Med 74 (4), 945–952. [PubMed: 25263499]

Zhang X, Cherry SR, Xie Z, Shi H, Badawi RD, Qi J, 2020 Subsecond total-body imaging using ultrasensitive positron emission tomography. Proc. Natl. Acad. Sci. U. S. A 117 (5), 2265–2267. [PubMed: 31964808]

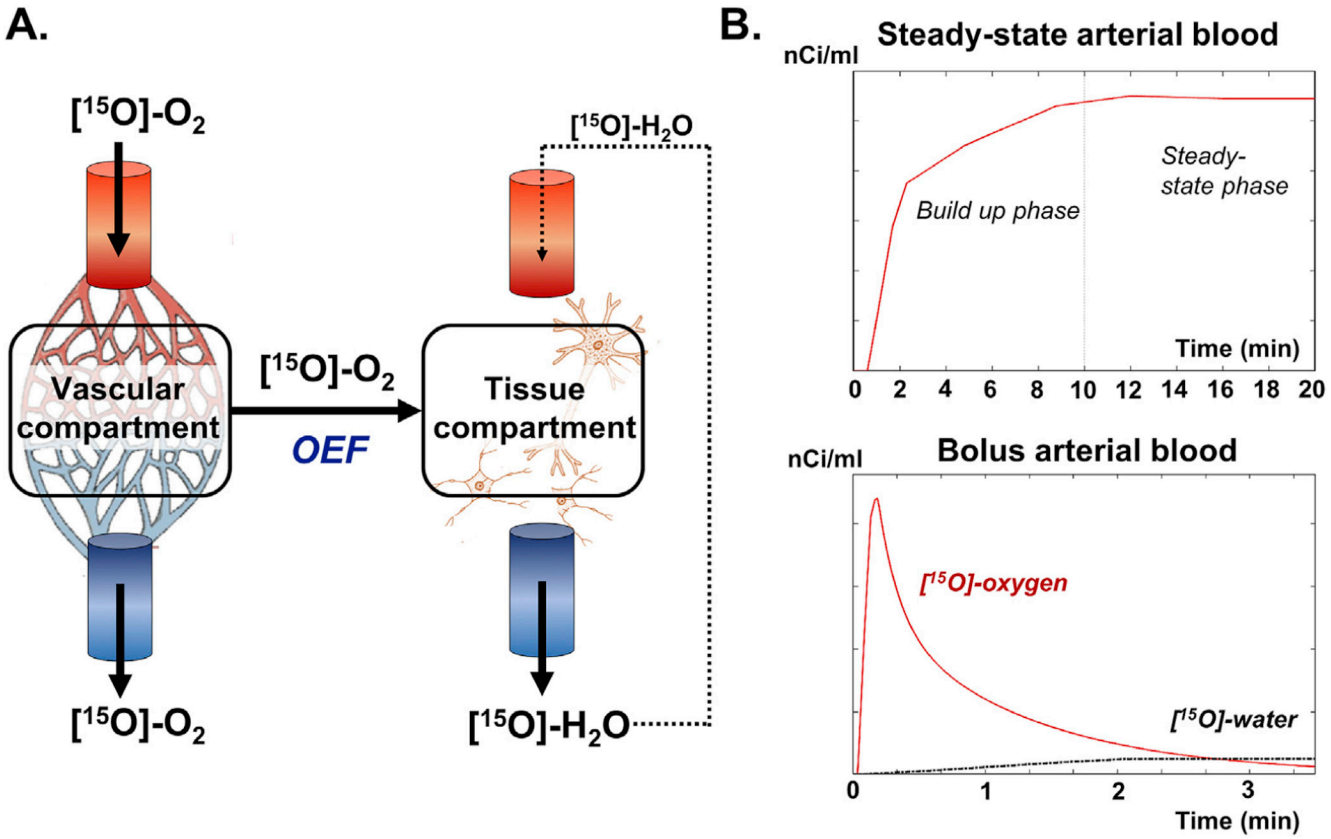

Fig. 1.

(a) One-tissue kinetic model (Mintun et al., 1984) of [^{15}O]-oxygen delivery through the blood circulation after inhalation, and uptake by cerebral tissues with oxygen extraction fraction (OEF). The dotted line indicates recirculation of the [^{15}O]-water metabolites through the bloodstream and is detected within the same PET voxels at later time points. (b) Red curves indicate example radioactivity time courses in arterial blood that is typically detected by invasive blood sampling in steady-state (equilibrium) and bolus inhalation [^{15}O]-oxygen studies. For bolus inhalation, the contribution of recirculating [^{15}O]-water to the PET signal is relevant primarily after 2–3 min of accumulation.

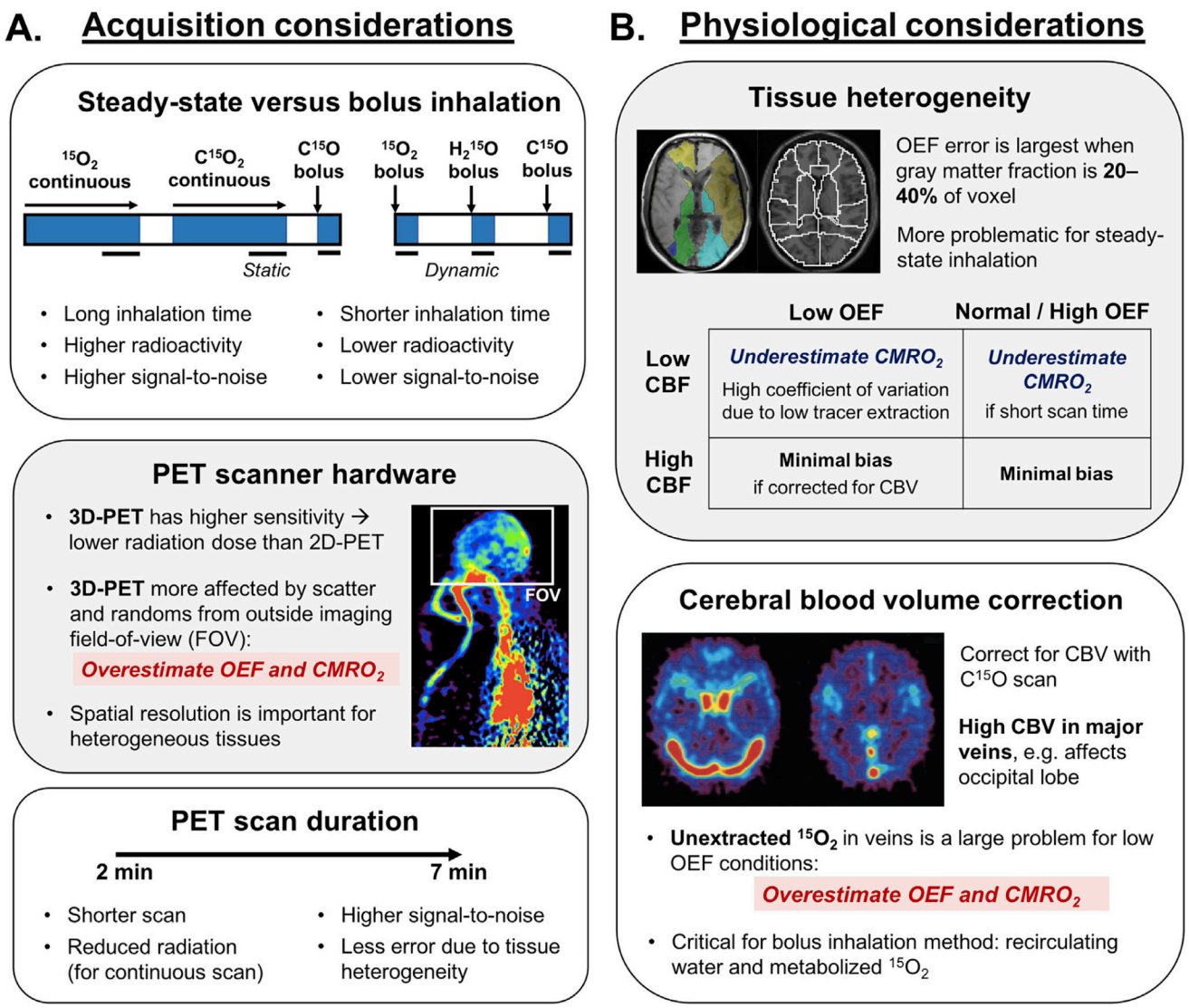

Fig. 2.

Schematic of PET imaging acquisition and physiological modeling considerations to accurately measure oxygen extraction fraction (OEF) and the cerebral metabolic rate of oxygen ($CMRO_2$) with [^{15}O]-oxygen PET. (a) Acquisition choices include steady-state (continuous) or bolus tracer administration; PET scan duration; and the imaging scanner hardware and reconstruction, including scatter correction (Hattori et al., 2004). (b) Physiological corrections include modeling of the tracer in the blood pool through a separate image of cerebral blood volume (Okazawa et al., 2001b). Tissue heterogeneity (Bremmer et al., 2011; Iguchi et al., 2018), i.e. the presence of multiple tissue types within a single voxel, is also a critical physiological concern especially for conditions of low perfusion and low OEF where comparatively little [^{15}O]-oxygen tracer is extracted.

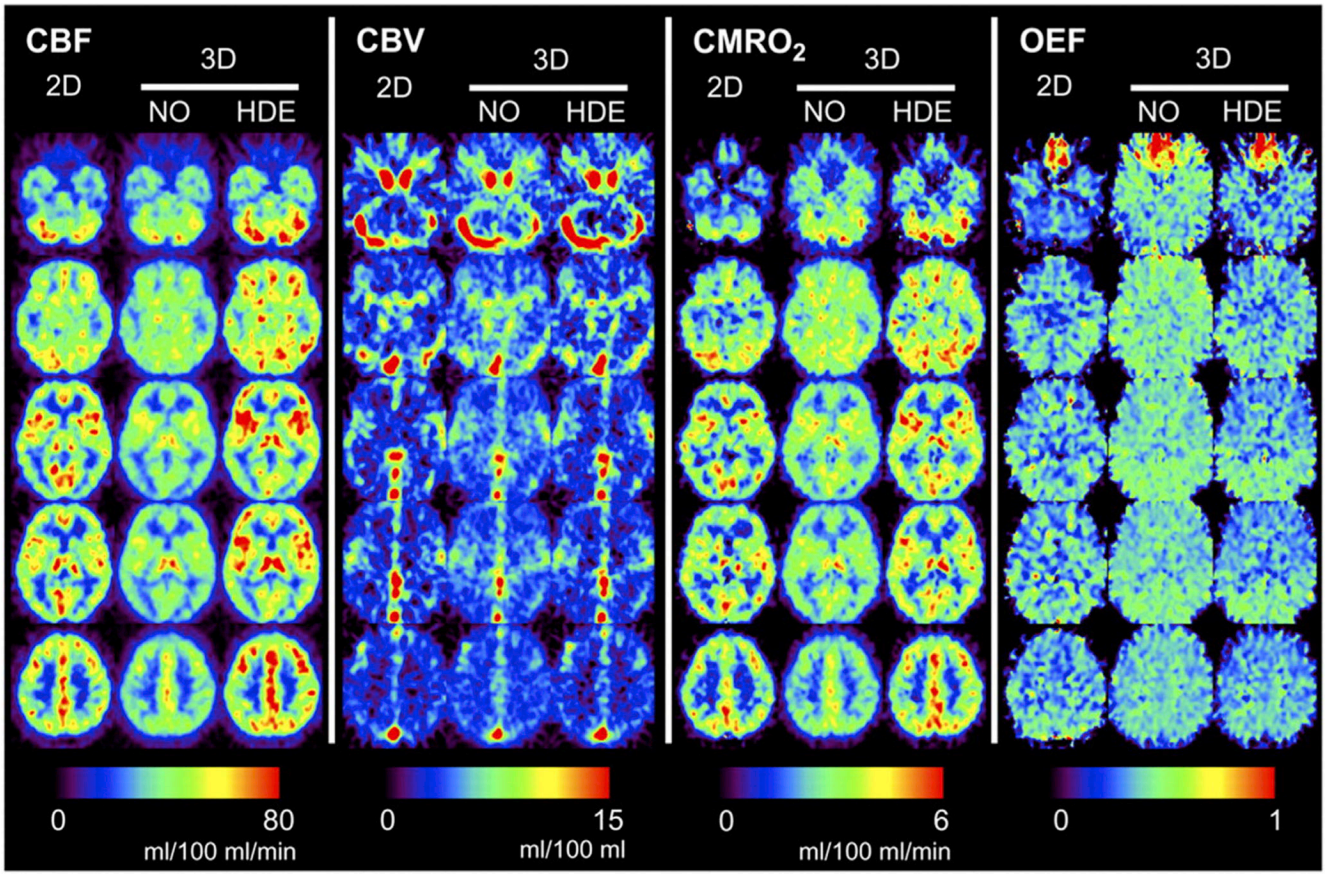

Fig. 3.

Comparison of hemodynamic maps from [^{15}O]-oxygen PET in the same heathy subject acquired with a 2D scanner; or a 3D scanner without scatter correction and with hybrid dual-energy (HDE) scatter correction. Differences between 2D PET and uncorrected 3D PET images were observed in 8 of 13 brain regions, but gray-to-white ratios of all parameters were consistent between 2D and 3D PET after scatter correction. This figure was originally published in Journal of Nuclear Medicine: Ibaraki et al., *J Nucl Med* 2008 (49): 50–59.

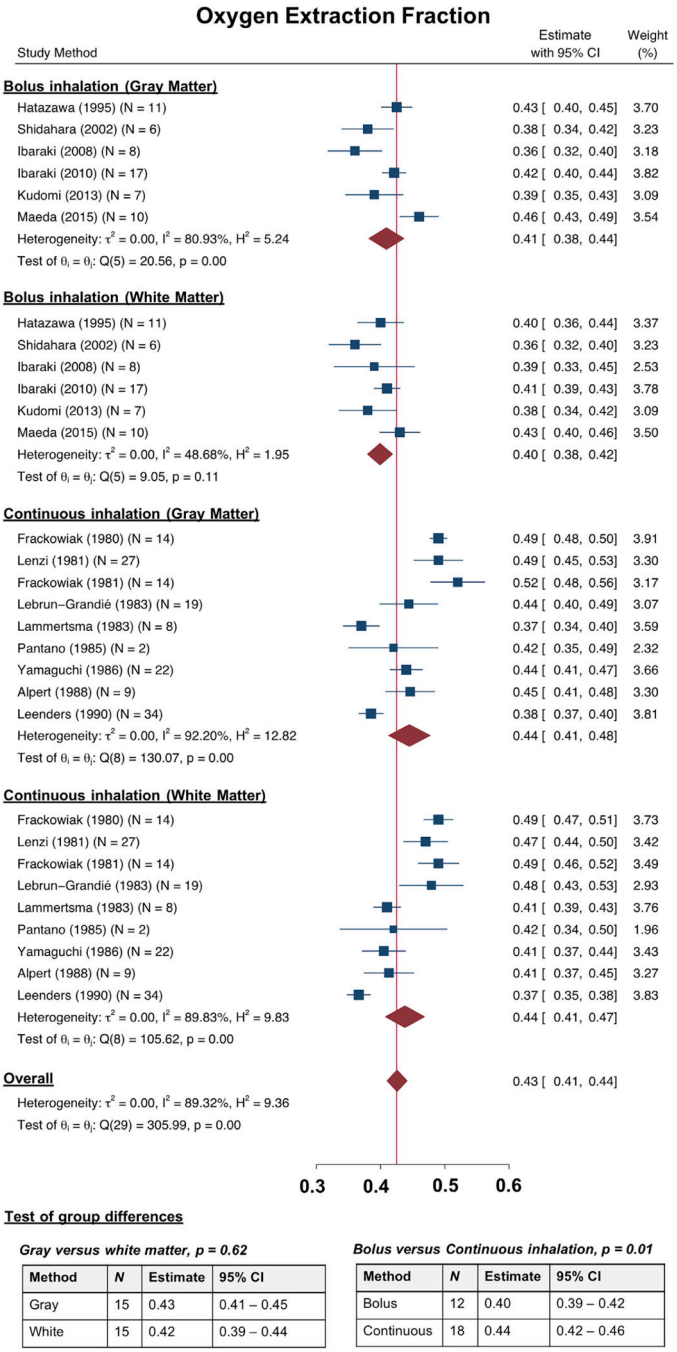

Fig. 4.

Forest plot illustrating random-effects meta-analysis and heterogeneity tests of oxygen extraction fraction (OEF) in healthy volunteers. OEF values are shown for gray and white matter regions, as measured by bolus-inhalation versus continuous-inhalation [^{15}O]-oxygen PET. Error bars account for sample size and the red diamonds indicate group averages. The τ^2 values are the between-study variances and the I^2 statistic reflects inconsistency across studies; a lower I^2 represents more consistency across studies. Test of group differences showed higher OEF values measured by steady-state PET than bolus inhalation PET.

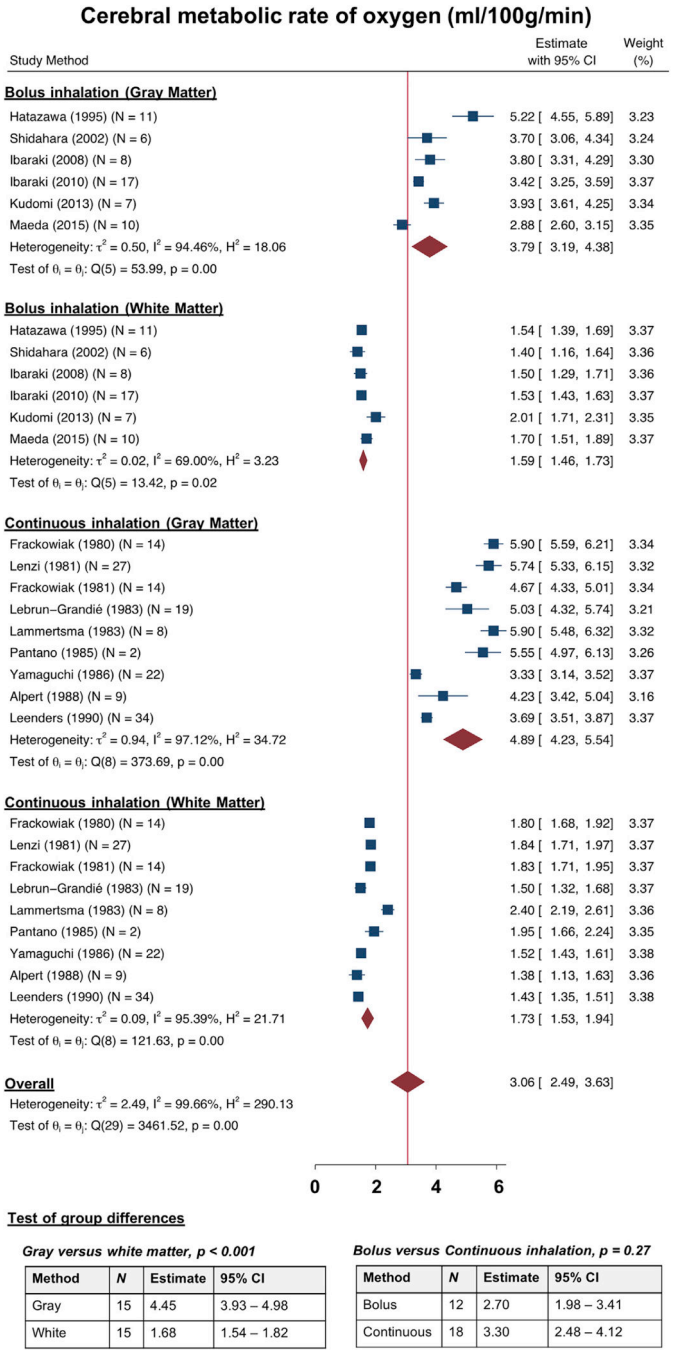

Fig. 5.

Forest plot illustrating random-effects meta-analysis and heterogeneity tests of cerebral metabolic rate of oxygen ($CMRO_2$) in healthy volunteers, delineated by gray and white matter and [^{15}O]-gas delivery method. Error bars account for sample size and the red diamonds indicate group averages. The τ^2 values are the between-study variances and the I^2 statistic reflects inconsistency across studies; a lower I^2 represents more consistency across studies. Gray matter $CMRO_2$ was larger than white matter $CMRO_2$. However, no significant

difference in $CMRO_2$ values was observed between bolus versus steady-steady PET methods.

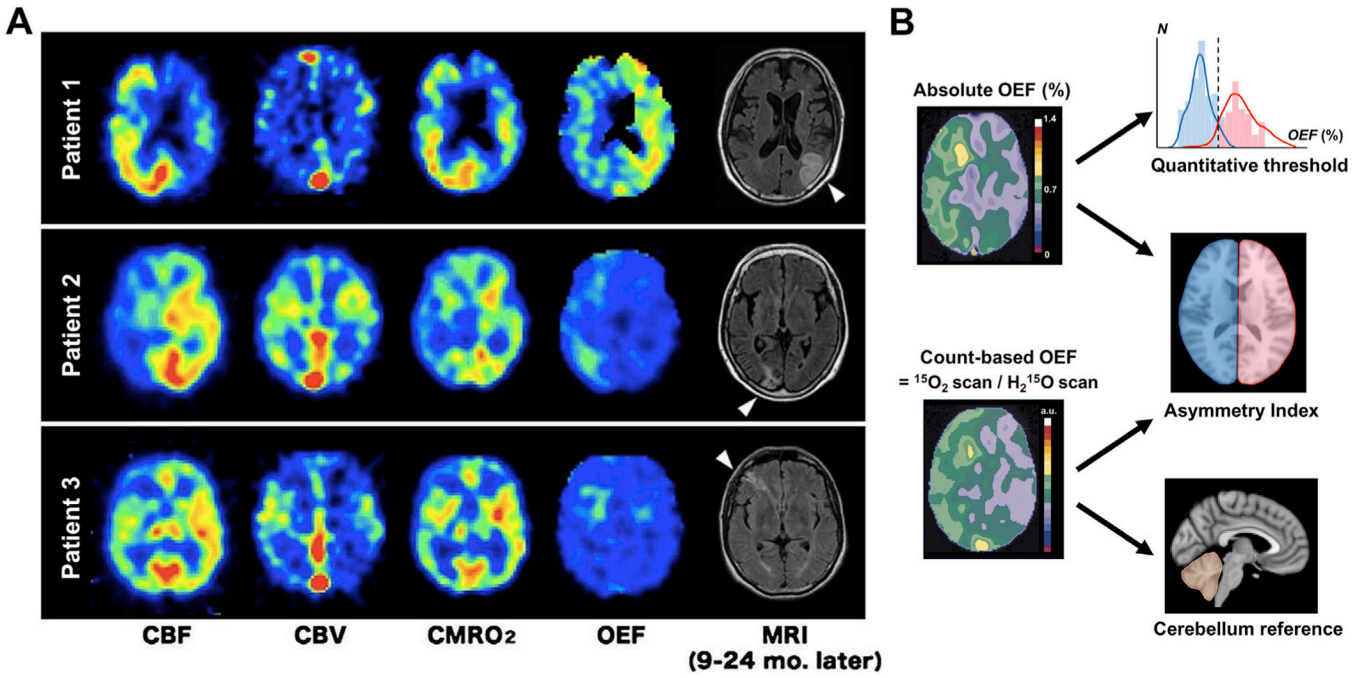

Fig. 6.

(a) Baseline hemodynamic images from [^{15}O]-oxygen PET in three patients with unilateral occlusive carotid artery disease. Focal areas of high absolute oxygen extraction fraction (OEF ranging from 0.51 to 0.58) corresponded to eventual lesion development on follow-up structural MRI after 9–24 months (arrowheads). Reproduced with permission from Hokari et al., *Surgical Neurology* 2009. (b) Schematic of different OEF metrics calculated from [^{15}O]-PET that have been used by clinical studies to identify hemodynamic impairment in cerebrovascular patients. Absolute threshold and an asymmetry index are two metrics to evaluate pathophysiology based on the underlying OEF map after kinetic modeling. Alternatively, an asymmetry index or normalized index (based on the cerebellum) can also be calculated based solely on the ratio of counts from the [^{15}O]-oxygen and [^{15}O]-water scans (Derdeyn et al., 2001). Adapted with permission from Derdeyn et al., *Radiology* 1999.

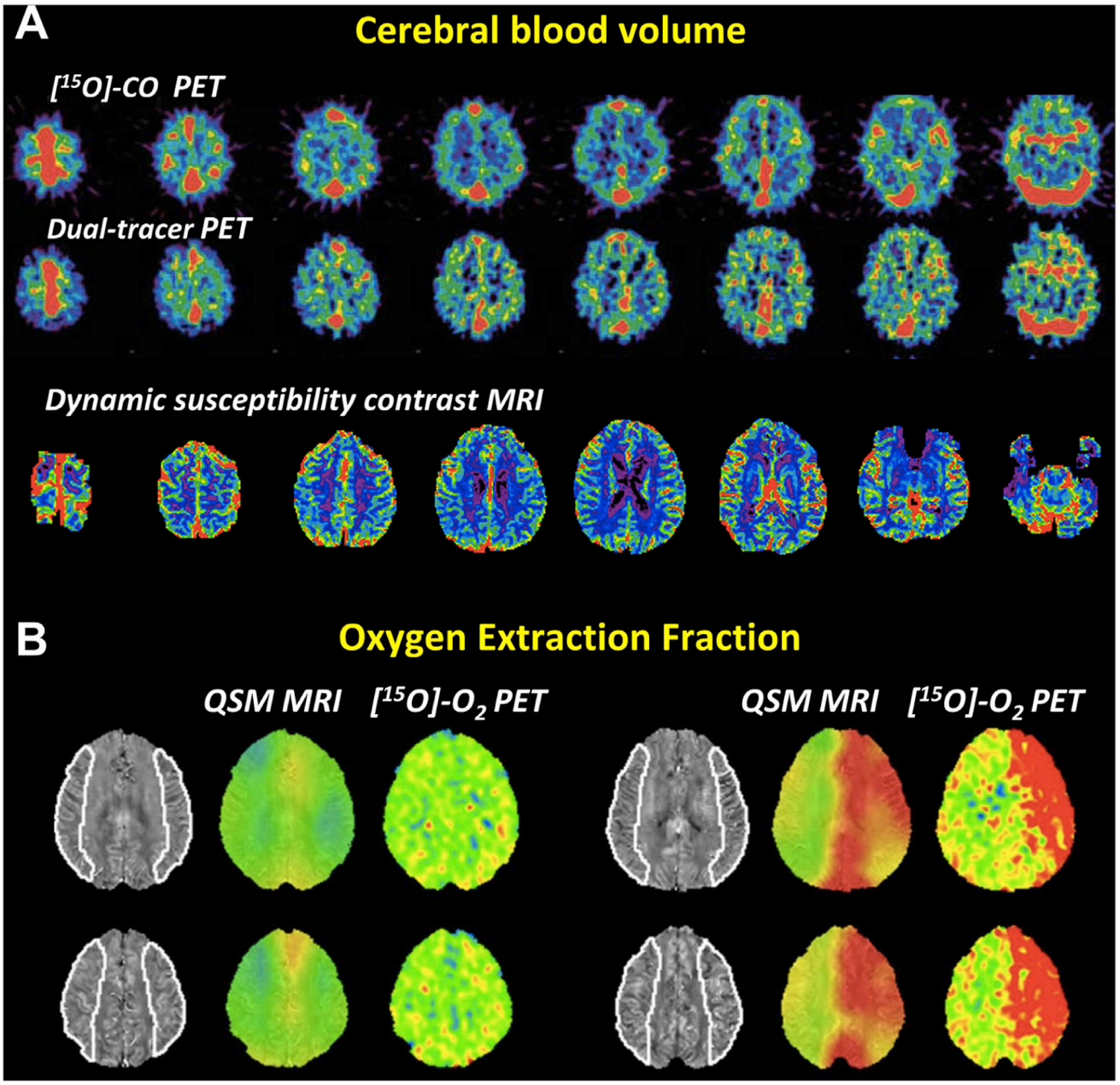

Fig. 7.

(a) Top and middle rows illustrate representative cerebral blood volume (CBV) maps quantified from [^{15}O]-CO PET in a healthy control and from fast, dynamic PET modeling with [^{15}O]-oxygen and [^{15}O]-water. The PET maps are reproduced with permission from Kudomi et al., *J Cereb Blood Flow Metab* 2013. Dynamic susceptibility contrast MRI maps of CBV after deconvolution with RAPID software is shown in a separate healthy volunteer for comparison and exhibits higher spatial resolution features in soft tissue. (b) Quantitative susceptibility mapping (QSM) MRI and [^{15}O]-oxygen PET reference images of oxygen extraction fraction in two patients with chronic ischemia. Structural MRI images have overlaid regions of interest in the middle cerebral artery territory. Good correspondence

between PET and MRI is observed in OEF asymmetry between the affected versus normal hemisphere of the patients. Figure is reproduced with permission from Uwano et al., *Stroke* 2017.

Table 1

Radiotracer dose ranges for [^{15}O]-gas PET scans.

Radiotracer	Measurement	Radioactivity dose (mCi)	Radioactivity dose (MBq)
[^{15}O]-oxygen (continuous inhalation)	Oxygen extraction fraction, oxygen metabolism	172–1400	6400[19]–51800[23]
[^{15}O]-oxygen (bolus inhalation)	Oxygen extraction fraction, oxygen metabolism	30–80	1110[27, 28]–3000[17, 25, 26]
[^{15}O]-CO_2 (continuous inhalation)	Cerebral blood flow	7.5–172	278[20]–6400[19]
[^{15}O]-H_2O (bolus inhalation)	Cerebral blood flow	15–40	555[30]–1480[38]
[^{15}O]-CO (bolus inhalation)	Cerebral blood volume	35–80	1300[37, 39]–3000[26]

Table 2

[^{15}O]-oxygen PET of brain OEF impairment in studies of cerebrovascular disease.

Study	Patient cohort	Number of patients	OEF threshold	Fraction of patients with impairment
Approach: Quantitative OEF values				
Yamauchi et al., *J Nucl Med* 1999 (Yamauchi et al., 1999)	Symptomatic stenosis or occlusion of ICA or MCA (>70%)	40	0.533	17.5%
Derdeyn et al., *J Nud Med* 2001 (Derdeyn et al., 2001)	Symptomatic athero-sclerotic ICA occlusion	68	0.590	48.5%
Okazawa et al., *EJNMMI* 2007 (Okazawa et al., 2007)	Unilateral steno-occlusion of major cerebral artery (>70%)	115	0.510	32.0%
Hokari et al., *J Nud Med* 2008 (Hokari et al., 2008)	Severe stenosis (>90%) or occlusion of ipsilateral ICA or MCA	65	0.500	22.1%
Hokari et al., *Surgical Neurology* 2009 (Hokari et al., 2009)	Severe stenosis (>90%) or occlusion of ipsilateral ICA or MCA	20	0.500	45.0%
Approach: Asymmetry index based on absolute OEF				
Powers et al., *Neurology* 1984 (Powers et al., 1984)	Symptomatic ICA steno-occlusive disease	17	1.08	11.8%
Powers et al., *Annals Internal Med* 1987 (Powers et al., 1987)	Unilateral stenosis of common carotid (>66%)	19	1.14	21.1%
Grubb et al., *JAMA* 1998 (Grubb et al., 1998) (STLCOS trial)	Symptomatic occlusion of one or both ICAs	81	1.08	48.1%
Derdeyn et al., *Am J Neuroradiol* 1998 (Derdeyn et al., 1998)	Symptomatic occlusion or stenosis of Ml segment of MCA	10	1.10	20.0%
Yamauchi et al., *J Nucl Med* 1999 (Yamauchi et al., 1999)	Symptomatic stenosis or occlusion of ICA or MCA (>70%)	40	1.09	35.0%
Derdeyn et al., *Radiology* 1999 (Derdeyn et al., 1999b)	Symptomatic athero-sclerotic ICA occlusion	68	1.08	45.6%
Ibaraki et al., *Ann Nucl Med* 2004 (Ibaraki et al., 2004)	Unilateral steno-occlusive disease of ICA or MCA (>80%)	6	1.20	16.7%
Okazawa et al., *EJNMMI* 2007 (Okazawa et al., 2007)	Unilateral steno-occlusion of major cerebral artery (>70%)	115	1.12	-
Kobayashi et al., *J Nucl Med* 2008 (Kobayashi et al, 2008)	Steno-occlusive disease (>70%) of ICA or MCA	25	1.17	12.0%
Chida et al., J Nucl Med 2011 (Chida etal., 2011)	Unilateral MCA or ICA occlusive disease (>50%)	34	1.09	18.6%
Kudo et al., *JCBFM* 2016 (Kudo et al., 2016)	Unilateral MCA or ICA steno-occlusive disease	26	1.09	30.8%
Uwano et al., *Stroke* 2017 (Uwano et al., 2017)	Unilateral MCA or ICA steno-occlusive disease	41	1.09	26.8%
Approach: Asymmetry index based on ratio of raw PET counts				
Grubb et al., *JAMA* 1998 (Grubb et al., 1998) (STLCOS trial)	Symptomatic occlusion of one or both ICAs	81	1.062	48.1%
Derdeyn et al., *Radiology* 1999 (Derdeyn et al., 1999b)	Symptomatic athero-sclerotic ICA occlusion	68	1.06	61.7%
Kobayashi et al., *J Nud Med* 2008 (Kobayashi et al., 2008)	Steno-occlusive disease (>70%) of ICA or MCA	25	1.12	12.0%
Jiang et al., *JCBFM* 2010 (Jiang et al., 2010)	Symptomatic athero-sclerotic ICA occlusion	33	1.07	47.4%

Study	Patient cohort	Number of patients	OEF threshold	Fraction of patients with impairment
Powers et al., *JAMA* 2011 (Powers et al., 2011) (COSS trial)	Symptomatic athero-sclerotic ICA occlusion	195	1.13	-
Approach: Normalization to cerebellum reference				
Ibaraki et al., *Ann Nucl Med* 2004 (Ibaraki et al., 2004)	Unilateral steno-occlusive disease of ICA or MCA (>80%)	6	1.21	-
Jiang et al., *JCBFM* 2010 (Jiang et al., 2010)	Symptomatic athero-sclerotic ICA occlusion	33	1.10	35.1%

COSS = Carotid Occlusion Surgery Study; ICA = internal carotid artery; MCA = middle cerebral artery; STLCOS = St. Louis Carotid Occlusion Study.